

1 Reply to comments, Referee #1

2 We would like to thank Referee #1 for his/her time, constructive and helpful comments, edits and suggestions.

3

4 **L42: 'give a MRD of  $-32.4 \pm (56.3) \%$ , . . . These results indicate that the IASI-NH<sub>3</sub> product performs**

5 **better than previous upper bound estimates (-50% - +100%).'**

6 **Really better? But  $-32.4\%-56.3\% < -50\%$ .**

7 The sentence did not entirely reflect the meaning. Former estimates were made on an expert guess basis/  
8 comparison with ground observations. The new estimate is the first which is fully based on column  
9 measurements and a better estimate of the performance of the product.

10

11 Line 42 changed to:

12 These results give an improved estimate of the IASI-NH<sub>3</sub> product performance compared to the previous upper  
13 bound estimates (-50% - +100%).

14

15

16 **L160: 'We excluded stations which have only retrieved or are believed to have, NH<sub>3</sub> total columns**

17 **smaller than. . .' However, those cases are also interesting to check for any overestimation of NH<sub>3</sub>**

18 **columns in the IASI dataset (many of the enhancements seen in Figure 1 in remote areas might be**

19 **artefacts.)**

20

21 We agree on this with the reviewer. However because of time restriction we chose to focus on this set of  
22 stations. Also we excluded high altitude stations located in regions with large variations of altitude, i.e.  
23 Jungfrauoch/Maido. The remaining possible stations/sites are mostly located in the arctic or Antarctic regions  
24 and not of direct interest to this study. All observations shown in Figure 1 were used as input in the comparison.

25

26 **L246: 'To account for the topography we only used observations which have at maximum an altitude**

27 **difference of 300 m between the location of the FTIR and the IASI pixel position.'**

28 **But this criterion does not allow to exclude all cases where there is a mountain between FTIR and IASI**

29 **measurement but still FTIR and IASI are at the same altitude. It should be extended also to the 'way'**

30 **between FTIR and IASI position. Can you exclude such a case?**

31

32 This is already the case, changed line 246 to:

33 To account for the topography we only used observations which have at maximum an altitude difference of 300  
34 m (in) between the location of the FTIR and the IASI pixel position.

35

36 **L253:**

37 **Please give the information whether the temporal criterion restricts the comparison dataset to the cases of**

38 **daytime IASI measurements.**

39

40 Only daytime measurements were used in this study, nighttime observations can be compared but the number of  
41 coinciding observations is very low due to the small number of nighttime observations (only during summers is  
42 the sun still high enough during the late evening ~local time 21.30). See line nr 128, where it was mentioned  
43 that we use the morning overpasses only.

44

45 **L275:**

46 **Please specify the source of the skin temperature together with its uncertainty.**

47 Source is the IASI L2 temperature profiles,

48

49 Added Line 276:

50 The Tskin temperatures are obtained from the IASI L2 temperature profiles which have an uncertainty of ~2 K  
51 at the surface (August et al., 2012).

52

53 Added reference:

54 August, T., Klaes, D., Schlüssel, P., Hultberg, T., Crapeau, M., Arriaga, A., O'Carroll, A., Coppens, D., Munro,  
55 R. and Calbet, X.: IASI on Metop-A: Operational Level 2 retrievals after five years in orbit, J. Quant. Spectrosc.  
56 Radiat. Transf., 113(11), 1340–1371, doi:10.1016/j.jqsrt.2012.02.028, 2012.

57

58 **L300:**

59 **To apply this method seems a bit strange since the satellite profile retrieval is not vertically resolved at**  
60 **all, but the FTIRs are. One should test how much the results change in case this method is not applied.**  
61 **Further, it should be possible to calculate a typical averaging kernel of the IASI retrievals by theoretical**  
62 **simulations.**

63 The effects are minor for most sites except for the stations with a large number of the IASI “sea” profile  
64 retrieved observations, i.e. for Wollongong and St. Denis.  
65 Typical averaging kernel; a typical averaging could be calculated, but the discussion remains to be about what is  
66 to be “typical”. Something more applicable would be multiple “typical” AVK cases depending on  
67 terrain/climate classes. Either way this would introduce more uncertainty instead of dealing/solving the current  
68 ones.

69  
70 **L407: ‘successful comparison’ It is not clear what ‘successful’ should mean here. Try to be more specific.**  
71 Removed the word “successful”

72  
73 **L462ff.: possible explanation for the negative bias of satellite data. Don’t one expect an underestimation**  
74 **of total columns from satellite mid-IR observations especially for gases with maxima very near to the**  
75 **surface due to the small thermal contrast there? The FTIR instruments, however, observe the entire**  
76 **columns. This difference would be included in case correct satellite averaging kernels could be used. This**  
77 **should be discussed more in detail.**

78  
79 This is true, however the exact effect cannot be estimated due to the variability of the sensitivity from  
80 observation to observation. A short section has been added to the discussion; from Line 491 onward:

81  
82 *Fourth, the negative bias of the satellite observations can be expected by the lack of sensitivity to concentrations*  
83 *near the surface. This is of course where the ammonia concentrations usually peak. The FTIR observations*  
84 *however do fully observe the lower layers in the troposphere thus causing a discrepancy. Normally one can*  
85 *correct for this using the averaging kernel of the satellite observations. However, the IASI-NH<sub>3</sub> retrieval does*  
86 *not produce an averaging kernel meaning it is not possible to calculate the exact effect. The use of a typical*  
87 *averaging kernel will cause more uncertainty as there is a large day to day variability in the averaging kernels*  
88 *as earlier retrievals showed (Clarisse et al., 2009).*

89  
90 **Fig. 6 and general:**  
91 **Both datasets, FTIR and satellite ones, seem to exclude negative values. Is this correct? If yes, how is it**  
92 **achieved (log-retrieval?) and should this not have an effect on the comparison for low column amounts?**  
93 The IASI-NH<sub>3</sub> retrieval does not retrieve negative total columns following the current retrieval procedure. In  
94 case of the FTIR retrieval it is possible to get negative values but due to the retrieval  
95 restrictions/settings/procedure it is uncommon. For the “per” station comparison a selection was made, as  
96 described in the manuscript, to only use the positive values, in principle this indeed effects the comparison for  
97 low column amounts and something like an outlier trim function would be more valid.

98  
99 Figure 5. Shifted the x- and y- limits to better show the negative values  
100 Figure 6. Added greyed values to show the selected and not selected values.

101  
102 **Technical:**

103 **L30-32:**  
104 **the term ‘observations’ appears 4 times, try to reformulate**

105 Changed Line 30-32;  
106 Line 30: daily observations to (bi-) daily overpasses.  
107 Line 31: surface observations to surface measurements.

108  
109 **L180 and throughout the manuscript: ‘60km’ -> ‘60 km’ blank between unit and number**  
110 Added a blank space to “ km “ in lines: L151, L182,L185, L359, L498, table 2, caption figure 3, figure 4, figure  
111 5, figure 6 and figure A1.

112 **Table 1 caption: ‘The topography described the typography of the region’ Please correct.**  
113 Changed part of Table 1 caption to: The topography describes the geography of the region surrounding the site.

114

115 Reply to comments, Referee #2

116 We would like to thank Referee #2 for his/her time, constructive and helpful comments, edits and suggestions.

117

118 **One overall point that should be stated clearly is that the IASI observation sensitivity is not taken into**  
119 **consideration in these comparisons given the IASI retrieval approach, which limits the information**  
120 **available to explain the differences seen between the IASI and the FTIR.**

121 This point was already shortly mentioned in section 2.3.2. We've added a section in the discussion following a  
122 comment of Referee nr 1. In addition, we would like to point out that the IASI retrieval product does come with  
123 uncertainty estimates which characterize IASI's sensitivity. These depend on the thermal contrast and total  
124 column of NH<sub>3</sub>. We decided to use a filter for on TC, which captures the main sensitivity component to prevent  
125 introducing any biases.

126

127

128 **1) Section 2.3.1: This section talks about the important spatial and temporal differences between the**  
129 **FTIR and IASI, which is very well done. However, due to the IASI retrieval approach the sometimes**  
130 **equally important vertical sampling difference are not taken into consideration. One sentence should be**  
131 **added stating that this difference cannot be determined due to the IASI retrieval and is thus ignored in**  
132 **this comparison.**

133

134 Line added to the end of the section: Vertical sampling differences are not taken into consideration in this study  
135 however the IASI selection criterion on the thermal contrast is conservative and only those measurements for  
136 which IASI has a good sensitivity to surface concentrations are selected.

137

138 **2) Line 246 change the “which” to a “that”.**

139

140 Changed as suggested.

141

142 **3) Section 2.3.2 lines 292-292: It might be more clear to the reader if the following was**  
143 **added to the end of the sentence, “The effect of the lack of the satellite averaging kernel**  
144 **is hard to predict so the satellite vertical sensitivity is not taken into consideration in this**  
145 **comparison.**

146

147 We have added: “... so the satellite vertical sensitivity is only taken into account through the selection criterion  
148 on the thermal contrast.”

149

150 **4) Also, in this section the authors provided a good response in regards to explaining where the x\_sat**  
151 **IASI profiles are coming from, however, this information was not explicitly added to the text. It would be**  
152 **good to add in some the response provided:**

153 **The IASI profiles are not fully retrieved profiles but the fixed shape profiles used as an assumption in the**  
154 **IASI retrieval, see Van Damme et al., 2015. These fixed profiles are used for scaling purposes to be able to**  
155 **account for the FTIR averaging kernel. Van Damme, M., Clarisse, L., Dammers, E., Liu, X., Nowak, J.**  
156 **B., Clerbaux, C., Flechard, C. R., Galy-Lacaux, C., Xu, W., Neuman, J. A., Tang, Y. S., Sutton, M. A.,**  
157 **Erisman, J. W., and Coheur, P. F.: Towards validation of ammonia (NH<sub>3</sub>) measurements from the IASI**  
158 **satellite, Atmos. Meas. Tech., 8, 1575-1591, doi:10.5194/amt-8-1575-2015, 2015.**

159 Sentence was added to line 296,

160 The IASI profiles are not fully retrieved profiles but fixed shape profiles used as an assumption in the IASI  
161 retrieval, see Van Damme et al., 2015a. These fixed profiles are used for scaling purposes to be able to account  
162 for the FTIR averaging kernel.

163

164 **5) It would be nice to added in the rationale for why total column averaging kernels were not used as**  
165 **discussed in your response. Just a simple statement acknowledging that total column AK could be used,**  
166 **but this should in principle be the same as the procedure used here . . .**

167 Line 297; added: A total column averaging kernel could be used instead, but in principle is similar to the  
168 procedure described here.

169

170 **6) Line 509: the reference “Shepherd” should be “Shephard” to match the reference list.**

171 Changed Shepherd to Shephard.

172



174 An evaluation of IASI-NH<sub>3</sub> with ground-based FTIR  
175 measurements

176 Enrico Dammers<sup>1</sup>, Mathias Palm<sup>2</sup>, Martin Van Damme<sup>1,3</sup>, Corinne Vigouroux<sup>4</sup>, Dan Smale<sup>5</sup>, Stephanie Conway<sup>6</sup>,  
177 Geoffrey C. Toon<sup>7</sup>, Nicholas Jones<sup>8</sup>, Eric Nussbaumer<sup>9</sup>, Thorsten Warneke<sup>2</sup>, Christof Petri<sup>2</sup>, Lieven Clarisse<sup>3</sup>,  
178 Cathy Clerbaux<sup>3</sup>, Christian Hermans<sup>4</sup>, Erik Lutsch<sup>6</sup>, Kim Strong<sup>6</sup>, James W. Hannigan<sup>9</sup>, Hideaki Nakajima<sup>10</sup>,  
179 Isamu Morino<sup>11</sup>, Beatriz Herrera<sup>12</sup>, Wolfgang Stremme<sup>12</sup>, Michel Grutter<sup>12</sup>, Martijn Schaap<sup>13</sup>, Roy J. Wichink  
180 Kruit<sup>14</sup>, Justus Notholt<sup>2</sup>, Pierre.-F. Coheur<sup>3</sup> and Jan Willem Erisman<sup>1,15</sup>

- 181 1. Cluster Earth and Climate, Department of Earth Sciences, Vrije Universiteit Amsterdam, Amsterdam, the  
182 Netherlands  
183 2. Institut für Umweltphysik, University of Bremen, Bremen, Germany  
184 3. Spectroscopie de l'Atmosphère, Service de Chimie Quantique et Photophysique, Université Libre de Bruxelles  
185 (ULB), Brussels, Belgium  
186 4. Royal Belgian Institute for Space Aeronomy (BIRA-IASB), Brussels, Belgium  
187 5. National Institute of Water and Atmosphere, Lauder, New Zealand  
188 6. University of Toronto, Toronto, Ontario, Canada  
189 7. Jet Propulsion Laboratory, California Institute of Technology, Pasadena  
190 8. University of Wollongong, Wollongong, Australia  
191 9. NCAR, Boulder, Colorado, United States  
192 10. Atmospheric Environment Division, National Institute for Environmental Studies (NIES), Japan  
193 11. National Institute for Environmental Studies, 16-2 Onogawa, Tsukuba, Ibaraki, 305-8506, Japan  
194 12. Centro de Ciencias de la Atmosfera, Universidad Nacional Autonoma de Mexico, Mexico City, Mexico  
195 13. TNO Built Environment and Geosciences, Department of Air Quality and Climate, Utrecht, the Netherlands  
196 14. National Institute for Public Health and the Environment (RIVM), Bilthoven, the Netherlands  
197 15. Louis Bolk Institute, Driebergen, the Netherlands

198  
199 *Correspondence to:* E. Dammers (e.dammers@vu.nl)

200 **Abstract.** Global distributions of atmospheric ammonia (NH<sub>3</sub>) measured with satellite instruments such as the  
201 Infrared Atmospheric Sounding Interferometer (IASI) contain valuable information on NH<sub>3</sub> concentrations and  
202 variability in regions not yet covered by ground based instruments. Due to their large spatial coverage and [\(bi-\)](#)  
203 [daily observations overpasses](#), the satellite observations have the potential to increase our knowledge of the  
204 distribution of NH<sub>3</sub> emissions, and associated seasonal cycles. However the observations remain poorly  
205 validated, with only a handful of available studies often using only surface [observations-measurements](#) without  
206 any vertical information. In this study, we present the first validation of the IASI-NH<sub>3</sub> product using ground-  
207 based Fourier Transform InfraRed (FTIR) observations. Using a recently developed consistent retrieval strategy,  
208 NH<sub>3</sub> concentration profiles have been retrieved using observations from nine Network for the Detection of  
209 Atmospheric Composition Change (NDACC) stations around the world between 2008- 2015. We demonstrate  
210 the importance of strict spatio-temporal collocation criteria for the comparison. Large differences in the  
211 regression results are observed for changing intervals of spatial criteria, mostly due to terrain characteristics and  
212 the short lifetime of NH<sub>3</sub> in the atmosphere. The seasonal variations of both datasets are consistent for most  
213 sites. Correlations are found to be high at sites in areas with considerable NH<sub>3</sub> levels, whereas correlations are  
214 lower at sites with low atmospheric NH<sub>3</sub> levels close to the detection limit of the IASI instrument. A  
215 combination of the observations from all sites (N<sub>obs</sub> = 547) give a MRD of  $-32.4 \pm (56.3) \%$ , a correlation  $r$  of  
216 0.8 with a slope of 0.73. [These results give an improved estimate of the IASI-NH<sub>3</sub> product performance](#)  
217 [compared to the previous upper bound estimates \(-50% - +100%\). These results indicate that the IASI NH<sub>3</sub>](#)  
218 [product performs better than previous upper bound estimates \(-50% - +100%\).](#)



220 **1. Introduction**

221 Humankind has increased the global emissions of reactive nitrogen to an unprecedented level (Holland et al.,  
222 1999; Rockström et al., 2009). The current global emissions of reactive nitrogen are estimated to be a factor four  
223 larger than pre-industrial levels (Fowler et al., 2013). Consequently atmospheric deposition of reactive nitrogen  
224 to ecosystems has substantially increased as well (Rodhe et al., 2002; Dentener et al., 2006). Ammonia (NH<sub>3</sub>)  
225 emissions play a major role in this deposition with a total emission of 49.3Tg in 2008 (Emission Database for  
226 Global Atmospheric Research (EDGAR), 2011). Although NH<sub>3</sub> emissions are predominantly from agriculture in  
227 the Northern Hemisphere, wildfires also play a role, with biomass burning contributing up to 8% of the global  
228 emission budget (Sutton et al., 2013). NH<sub>3</sub> has been shown to be a major factor in the acidification and  
229 eutrophication of soil and water bodies, which threatens biodiversity in vulnerable ecosystems (Bobbink et al.,  
230 2010; Erisman et al., 2008, 2011). Through reactions with sulphuric and nitric acid, NH<sub>3</sub> also contributes to the  
231 formation of particulate matter which is associated with adverse health effects (Pope et al., 2009). Particulate  
232 ammonium salts contribute largely to aerosol loads over continental regions (Schaap et al., 2004). Through its  
233 role in aerosol formation, NH<sub>3</sub> also has an impact on global climate change as hygroscopic ammonium salts are  
234 of importance for the aerosol climate effect and thus the global radiance budget (Adams et al., 2001).  
235 Furthermore increased NH<sub>3</sub> concentrations in the soil also enhance the emission of nitrous oxide (N<sub>2</sub>O) which is  
236 an important greenhouse gas and an ozone-depleting substance (Ravishankara et al., 2009). Finally nitrogen  
237 availability is a key factor for the fixation of carbon dioxide (CO<sub>2</sub>) and thus it is an important factor in climate  
238 change.  
239

240 Despite the fact that NH<sub>3</sub> at its current levels is a major threat to the environment and human health, relatively  
241 little is known about its total budget and global distribution (Sutton et al., 2013; Erisman et al., 2007). Surface  
242 observations are sparse and mainly available for north-western Europe, the United States and China (Van  
243 Damme et al., 2015a). At the available sites, in situ measurements are mostly performed with relatively poor  
244 temporal resolution due to the high costs of performing reliable NH<sub>3</sub> measurements with high temporal  
245 resolution. These measurements of NH<sub>3</sub> are also hampered by sampling artefacts caused by the reactivity of NH<sub>3</sub>  
246 and the evaporation of ammonium nitrate (Slanina et al., 2001; von Bobrutzki et al., 2010; Puchalski et al.,  
247 2011). As the lifetime of atmospheric NH<sub>3</sub> is rather short, on the order of hours to a few days, due to efficient  
248 deposition and fast conversion to particulate matter, the existing surface measurements are not sufficient to  
249 estimate global emissions without inducing large errors. The lack of vertical profile information further hampers  
250 the quantification of the budget, with only a few reported airborne measurements (Nowak et al., 2007, 2010,  
251 Leen et al., 2013, Whitburn et al., 2015).

252 Advanced IR-sounders such as the Infrared Atmospheric Sounding Interferometer (IASI), the Tropospheric  
253 Emission Spectrometer (TES), and the Cross-track Infrared Sounder (CrIS) enable retrievals of atmospheric  
254 NH<sub>3</sub> (Beer et al., 2008; Coheur et al., 2009; Clarisse et al., 2009; Shephard et al., 2011, 2015a). The availability  
255 of satellite retrievals provide a means to consistently monitor global NH<sub>3</sub> distributions. Global distributions  
256 derived from IASI and TES observations have shown high NH<sub>3</sub> levels in regions not covered by ground-based  
257 data. In this way, more insight was gained into known and unknown NH<sub>3</sub> sources worldwide including biomass  
258 burning, industry and agricultural areas. Hence, satellite observations have the potential to improve our

259 knowledge of the distribution of global emissions and their seasonal variation due to their large spatial coverage  
260 and (bi-) daily observations (Zhu et al., 2013; Van Damme et al., 2014b, 2015b; Whitburn et al., 2015; Luo et  
261 al., 2015). However, the satellite observations remain poorly validated with only a few dedicated campaigns  
262 performed with limited spatial, vertical or temporal coverage (Van Damme et al., 2015a; Shephard et al., 2015b,  
263 Sun et al., 2015).

264 Only a few studies have explored the quality of the IASI-NH<sub>3</sub> product. A first evaluation of the IASI  
265 observations was made over Europe using the LOTOS-EUROS model and has shown the respective consistency  
266 of the measurements and simulations (Van Damme et al., 2014b). A first comparison using ground-based and  
267 airborne measurements to validate the IASI-NH<sub>3</sub> data set were made in Van Damme et al. (2015a). They  
268 confirmed consistency between the IASI-NH<sub>3</sub> data set and the available ground-based observations and showed  
269 promising results for validation by using independent airborne data from the CalNex campaign. Nevertheless,  
270 that study was limited by the availability of independent measurements and suffered from representativeness  
271 issues for the satellite observations when comparing to surface concentration measurements. One of the key  
272 conclusions was the need for vertical profiles (e.g. ground-based remote sensing products or upper-air in situ  
273 measurements to compare similar quantities). Recently, Dammers et al. (2015) developed a retrieval  
274 methodology for Fourier Transform Infrared Spectroscopy (FTIR) instruments to obtain remotely sensed  
275 measurements of NH<sub>3</sub> and demonstrated the retrieval characteristics for four sites located in agricultural and  
276 remote areas. Here we explore the use of NH<sub>3</sub> total columns obtained with ground based FTIR at nine stations  
277 with a range of NH<sub>3</sub> pollution levels to validate the IASI-NH<sub>3</sub> satellite product by Van Damme (2014a).

278 First, we concisely describe the ground based FTIR retrieval and IASI-NH<sub>3</sub> product datasets in Sections 2.1 and  
279 2.2. Next we describe the methodology of the comparison in Section 2.3 followed by the presentation of the  
280 results in Section 3, which are then summarized and discussed in Section 4.

281



282 **2. Description of the satellite and FTIR data sets and validation methodology**

283 **2.1 IASI-NH<sub>3</sub> product**

284 The first global NH<sub>3</sub> distribution was obtained by a conventional retrieval method applied to IASI spectra  
285 (Clarisse et al., 2009), followed by an in depth case study, using a more sophisticated algorithm, of the  
286 sounder's capabilities depending on the thermal contrast (defined in Van Damme et al. (2014a) as the  
287 temperature differences between the Earth surface and the atmosphere at 1.5 km altitude, Clarisse et al., 2010).  
288 In this study we use the NH<sub>3</sub> product developed by Van Damme et al. (2014a). Their product is based on the  
289 calculation of a dimensionless spectral index (Hyperspectral Range Index: HRI), which is a quantity  
290 representative of the amount of NH<sub>3</sub> in the total atmospheric column. This HRI is then converted into NH<sub>3</sub> total  
291 columns using look-up-tables based on numerous forward simulations for various atmospheric conditions.  
292 These look-up-tables relate the HRI and the thermal contrast to a total column of NH<sub>3</sub> (Van Damme et al.,  
293 2014a). The product includes an error characterization of the retrieved column based on errors in the thermal  
294 contrast and HRI. Important advantages of this method over the method by Clarisse (2009) is the relatively  
295 small computational cost, the improved detection limit and the ability to identify smaller emission sources and  
296 transport patterns above the sea. One of the limitations of this method is the use of only two NH<sub>3</sub> vertical  
297 profiles: a "source profile" for land cases and a "transported profile" for sea cases (Illustrated in Van Damme et  
298 al., 2014a, fig. 3). Another limitation of the product is that it does not allow the calculation of an averaging  
299 kernel to account for the vertical sensitivity of the instrument sounding to different layers in the atmosphere. In  
300 this paper we will use NH<sub>3</sub> total columns retrieved from the IASI-A instrument (aboard of the MetOp-A  
301 platform) morning overpass (AM) observations (i.e. 09:30 local time at the equator during overpass) which have  
302 a circular footprint of 12 km diameter at nadir and an ellipsoid shaped footprint of up to 20 km x 39 km at the  
303 outermost angles. We will use observations from January 1<sup>st</sup> 2008 to December 31<sup>st</sup> 2014. Figure 1 shows the  
304 mean IASI-NH<sub>3</sub> total column distribution (all observations gridded to a 0.1° x 0.1° grid) using observations  
305 above land for the years 2008-2014. The mean columns are obtained through a weighting with the relative error  
306 (see Van Damme et al., 2014). The bottom left inset shows the corresponding relative error.

307

308

## 309 2.2 FTIR- NH<sub>3</sub> retrieval

310  
311 The FTIR-NH<sub>3</sub> retrieval methodology used here is described in detail in Dammers et al. (2015) and a summary  
312 is given here. The retrieval is based on the use of two spectral micro-windows, which contain strong individual  
313 NH<sub>3</sub> absorption lines. The two spectral windows [930.32-931.32 cm<sup>-1</sup>, MW1] and [962.70-970.00 cm<sup>-1</sup>, MW2]  
314 or the wider version for regions with very low concentrations [929.40-931.40 cm<sup>-1</sup>, MW1 Wide] and [962.10-  
315 970.00 cm<sup>-1</sup>, MW2 Wide] are fitted using SFIT4 (Pougatchev et al., 1995; Hase et al., 2004, 2006) or a similar  
316 retrieval algorithm (Hase et al, 1999) based on the optimal estimation method (Rodgers et al., 2000) to retrieve  
317 the volume mixing ratios (in ppbv) and total columns of NH<sub>3</sub> (in molecules cm<sup>-2</sup>). Major interfering species in  
318 these windows include H<sub>2</sub>O, CO<sub>2</sub> and O<sub>3</sub>. Minor interfering species are N<sub>2</sub>O, HNO<sub>3</sub>, CFC-12 and SF<sub>6</sub>. For the  
319 line spectroscopy, the HITRAN 2012 (Rothman et al., 2013) database is used with a few adjustments for CO<sub>2</sub>  
320 (ATMOS, Brown et al., 1996), and sets of pseudo-lines generated by NASA-JPL (G.C. Toon) are used for the  
321 broad absorptions by heavy molecules (i.e. CFC-12, SF<sub>6</sub>). The *a-priori* profiles of NH<sub>3</sub> are based on balloon  
322 measurements (Toon et al., 1999) and scaled to fit common surface concentrations at each of the sites. An  
323 exception is made for the *a-priori* profile at Reunion Island where a modelled profile from the MOZART model  
324 is used (Louisa Emmons, personal communication, 2014). There, the profile peaks at a height of 4-5 km, as NH<sub>3</sub>  
325 are expected to be due to transport of biomass burning emissions on the island and Madagascar. For all stations,  
326 the *a-priori* profiles for interfering species are taken from the Whole Atmosphere Community Climate Model  
327 (WACCM, Chang et al., 2008). Errors in the retrieval are typically ~30% (Dammers et al., 2015), which are  
328 mostly due to uncertainties in the spectroscopy in the line intensities of NH<sub>3</sub> and the temperature and pressure  
329 broadening coefficients (HITRAN 2012).

330  
331 An effort has been made to gather observations from most of the station part of the Network for the Detection of  
332 Atmospheric Composition Change (NDACC) which have obtained relevant solar spectra between 1<sup>st</sup> of Jan  
333 2008 and 31<sup>st</sup> of Dec 2014. We excluded stations which have only retrieved or are believed to have, NH<sub>3</sub> total  
334 columns smaller than 5x10<sup>15</sup> (molecules cm<sup>-2</sup>) during the study interval (i.e. Arctic and Antarctic and other  
335 stations with concentrations below the expected limits of the IASI-NH<sub>3</sub> product, at best ~5x10<sup>15</sup> for observations  
336 with high thermal contrast). Figure 1 shows the positions of the FTIR stations used in this study. The retrieved  
337 NH<sub>3</sub> total columns (molecules cm<sup>-2</sup>) for each of the stations are shown in Figure 2. The number of available  
338 observations per station varies as does the range in total columns with high values of ~100x10<sup>15</sup> (molecules cm<sup>-2</sup>)  
339 observed at Bremen and low values of about 1x10<sup>15</sup> (molecules cm<sup>-2</sup>) at St Denis Reunion. The following  
340 provides a short description of each of the sites used in this study and retrieved NH<sub>3</sub> columns (molecules cm<sup>-2</sup>).  
341 Additionally, a short summary can be found in Table 1:

342 The **Bremen** site operated on the university campus by the University of Bremen in the northern part of the city  
343 (Velazco et al., 2007). Bremen is located in the northwest of Germany, which is characterized by intensive  
344 agriculture. It is most suitable for comparisons with IASI given the very high observed concentrations (Fig. 2,  
345 blue) and flat geography surrounding the station. NH<sub>3</sub> sources near the measurement station include manure  
346 application to fields, livestock housing and exhaust emissions of local traffic. The retrieved NH<sub>3</sub> total columns  
347 peak in spring due to manure application and show an increase in summer due to increased volatilization of NH<sub>3</sub>  
348 from livestock housing and fields when temperatures increase during summer.

349 The **Toronto** site (Wiacek et al., 2007) is located on the campus of the University of Toronto, Canada. The city  
350 is next to Lake Ontario with few sources to the south. NH<sub>3</sub> sources are mainly due to agriculture as well as local  
351 traffic in the city. Occasionally, NH<sub>3</sub> in smoke plumes from major boreal fires to the north and west of the city  
352 can be observed (Lutsch et al., 2016). The retrieved columns (Fig. 2, green) show increased values during  
353 summers as well as peaks in spring.

354 The **Boulder** observation site is located at the NCAR Foothills Lab in Boulder, Colorado, United States of  
355 America, about 60 km northwest of the large metropolitan Denver area. It is located at 1.6 km a.s.l. on the  
356 generally dry Colorado Plateau. Directly to the west are the foothills of the Rocky Mountain range and to the  
357 east are rural grasslands, farming and ranching facilities. Among them are large cattle feed lots to the northeast  
358 near Greeley approximately 90 km distant. The area is subject to occasional seasonal local forest fires and also  
359 occasionally sees plumes from fires as distant as Washington or California. The retrieved columns (Fig. 2, grey)  
360 show the largest increase during summers.

361 The **Tsukuba** site (Ohyama et al., 2009) is located at the National Institute for Environmental Studies (NIES),  
362 in Japan. The region is a mixture of residential and rural zones with mountains to the north. NH<sub>3</sub> sources near  
363 the measurement site include manure and fertilizer applications and exhaust emissions of local traffic in the  
364 surrounding city with a large part originating from the from the Tokyo metropolitan area. The retrieved columns  
365 (Fig 2, red) show a general increase during the summers due to increased volatilization rates.

366 The **Pasadena** site lies on the Northern edge of the Los Angeles conurbation in the United States of America, at  
367 the foot of the San Gabriel mountains which rise steeply to the north to over 1.5 km altitude within 5 km  
368 distance. Local sources of NH<sub>3</sub> include traffic, livestock, and occasional fires. FTIR observations typically take  
369 place around local noon to avoid solar obstruction by nearby buildings and morning stratus cloud that is  
370 common May-July. The highest retrieved columns (Fig.2, cyan) are observed during the summers.

371 The **Mexico City** site is located on the campus of the National Autonomous University of Mexico (UNAM) at  
372 2280 m a.s.l., south of the metropolitan area. Surface NH<sub>3</sub> concentrations were measured by active open-path  
373 FTIR during 2003 with typical values between 10 - 40 ppb (Moya et al. 2004). The megacity is host to more  
374 than 22 million inhabitants, over 5 million motor vehicles and a wide variety of industrial activities. Low  
375 ventilation during night and morning causes an effective accumulation of the NH<sub>3</sub> and other pollutants in  
376 Mexico City, which is located in a flat basin surrounded by mountains. The concentration and vertical  
377 distribution of pollutants are dominated by the large emissions and the dynamics of the boundary layer which is  
378 on average 1.5 km height during the IASI morning overpass (Stremme et al., 2009, 2013). The retrieved  
379 columns (Fig.2, orange) show an increase during the summers as well as a large daily variation.

380 The measurement site on the university campus of **St.-Denis** (Senten et al., 2008) is located on the remote  
381 Reunion Island in the Indian Ocean. Observed NH<sub>3</sub> columns (Fig. 2, purple) are usually low due to the lack of  
382 major sources nearby the site but increases are observed during the fire season (Sept.-Nov.) with possible fire  
383 plumes originating from Madagascar, as already observed in another study involving short-lived species  
384 (Vigouroux et al., 2009). Local NH<sub>3</sub> emissions include fertilizer applied for sugar cane production and local  
385 biomass burning.

386 The **Wollongong** site is located on the campus of the University of Wollongong. The city of Wollongong is on  
387 the south east coast of Australia with the University only about 2.5 km from the ocean. The measurement site is  
388 also influenced by a 400m escarpment 1 km to the West, and the city of Sydney 60 km to the north. NH<sub>3</sub>

389 sources come mainly from city traffic, as well as seasonal forest fires that can produce locally high amounts of  
390 smoke and subsequent NH<sub>3</sub> emissions (Paton-Walsh et al., 2005). The retrieved columns (Fig.2, brown) peak  
391 during the summer season due to the higher temperatures and seasonal forest fires.

392 The **Lauder** (Morgenstern et al., 2012) National Institute of Water and Atmospheric Research (NIWA) station  
393 in Central Otago, New Zealand, is located in a hilly region with NH<sub>3</sub> emissions in the valley surrounding the  
394 station mostly due to livestock grazing and fertilizer application. The observed columns (Fig. 2, black) show a  
395 general increase during summers due to increased volatilization rates.

396

397

398 **2.3 FTIR and satellite comparison methodology**

399 **2.3.1 Co-location & data criteria**

400

401 NH<sub>3</sub> is highly variable in time and space which complicates the comparison between the IASI and FTIR  
402 observations. Therefore collocation criteria were developed to investigate and mitigate the effect of the spatial  
403 and temporal differences between the FTIR and IASI observations on their correlation. So far, there is no model  
404 to describe the representativeness of a site for the region so a simple criterion was initially derived by analyzing  
405 the terrain around each site and comparing the correlation of the IASI and FTIR observations for multiple time  
406 and spatial differences to find the best correlation. To illustrate the differences between the representativeness of  
407 the sites we take the stations at Bremen, Lauder and Wollongong as examples. Around Bremen the terrain is flat  
408 with high reported NH<sub>3</sub> emissions (Kuenen et al., 2014) in the region surrounding the city. In contrast, Lauder is  
409 located in a hilly region with low NH<sub>3</sub> emissions mostly due to local livestock grazing and fertilizer application  
410 in the surrounding valleys (EDGAR, 2011). Owing to the flat terrain, the region around Bremen should, in  
411 principle, have more homogeneous concentrations than Lauder. A more extreme case for geographical  
412 inhomogeneity is Wollongong. Wollongong is located at the coast near a 400m escarpment without major  
413 nearby NH<sub>3</sub> sources. Hence increasing distances between the satellite measurement pixel center and the station  
414 may negatively impact the comparison due to the short lifetime of NH<sub>3</sub>, and the limitation on transport of NH<sub>3</sub>  
415 to the site by the terrain (i.e. representativeness problems). Because no uniform criterion was found that would  
416 enable a good comparison for all stations, multiple criteria with a maximum difference of between 10 km and 50  
417 km will be used to analyze the optimal setting for each of the sites. Vertical sampling differences are not taken  
418 into consideration in this study however the IASI selection criterion on the thermal contrast is conservative  
419 and only those measurements for which IASI has a good sensitivity to surface concentrations are selected.

420

421 **Topography**

422 Any hill or mountain range located between the satellite pixel and the FTIR station may inhibit transport and  
423 decrease their comparability. To account for the topography we only used observations ~~which that~~ have at  
424 maximum an altitude difference of 300 m (in) between the location of the FTIR and the IASI pixel position. The  
425 300 m criterion was chosen based on tests using the FTIR and satellite observations from Lauder. For the  
426 calculation of the height differences we used the Space Shuttle Radar Topography Mission Global product at 3  
427 arc second resolution (SRTMGL3, Farr et al., 2007).

428

429 **Temporal variation**

430 NH<sub>3</sub> concentrations can vary considerably during the day, with lifetimes as short as a few hours not being  
431 uncommon (Dentener and Crutzen, 1994; Bleeker et al., 2009). The variability of the concentrations mainly  
432 arises from the variability in emission strengths as influenced by agricultural practices, meteorological, and  
433 atmospheric conditions such as temperature, precipitation, wind speed and direction, the development of the  
434 boundary layer (which is important as the IASI satellite observations take place around 9.30 local time and thus  
435 the boundary layer has not always been fully established), pollution level, and deposition rates. To minimize the  
436 effects of this variability on the comparability of the IASI and FTIR observations, satellite observations with a  
437 time difference to FTIR observation of no more than 90 minutes were used.

438

439 **Product error**

440 The error of the IASI-NH<sub>3</sub> columns derives from errors on the HRI and the thermal contrast (Van Damme et al.,  
441 2014a). Applying relative error filters of 50, 75 and 100% showed that mostly lower concentrations are removed  
442 from the comparison. Consequently, introducing any criteria based on the associated (relative) error will bias  
443 any comparison with FTIR columns towards the higher IASI total columns. Therefore, we decided not to filter  
444 based on the relative error as it skews the range of NH<sub>3</sub> column totals.

446 **Meteorological factors**

447 The lowest detectable total column of the retrieval depends on the thermal contrast of the atmosphere (Van  
448 Damme et al., 2014a). For example, the retrieval has a minimum detectable NH<sub>3</sub> column of around  $5 \times 10^{15}$   
449 molecules cm<sup>-2</sup> at a thermal contrast of about 12 Kelvin (K) for columns using the “transported” profile. A  
450 thermal contrast of 12 K is chosen as the threshold to ensure the quality of the IASI observations, which  
451 represents a lapse rate of around 8K/km altitude, near standard atmospheric conditions. We excluded data for  
452 T<sub>skin</sub> temperatures below 275.15 K to introduce a basic filter for snow cover and conditions with frozen soils.

453 The T<sub>skin</sub> temperatures are obtained from the IASI L2 temperature profiles which have an uncertainty of ~2 K at  
454 the surface (August et al., 2012). Finally, only IASI observations with a cloud cover below 10% are used.

Formatted: Subscript

456 The complete list of selection criteria is summarized in Table 2.

458 **Quality of the FTIR observations**

459 No filters were applied to maximize the number of observations usable in the comparison. The resolution and  
460 detection limit of the FTIR instruments is usually better than that of the IASI instrument, leading to retrieved  
461 columns with, in principle, less uncertainty. Overall the FTIR retrievals show an error of ~30% or less with the  
462 largest errors due to the spectroscopic parameters (Dammers et al., 2015). While artefacts are possible in the  
463 data we did not investigate for specific artefacts and possible impacts.

466 **2.3.2 Application of averaging kernels**

467 When performing a direct comparison between two remote sensing retrievals, one should take into account the  
468 vertical sensitivity and the influence of a-priori profiles of both methods. One method to remove the influence of  
469 the a-priori profile and the vertical sensitivity is the application of the averaging kernels of both retrievals to the  
470 retrieved profiles of both products. The IASI-NH<sub>3</sub> HRI-based product scheme however, does not produce  
471 averaging kernels thus it is not possible to account for the vertical sensitivity of the satellite retrieval. The effect  
472 of the lack of the satellite averaging kernel is hard to predict, so the satellite vertical sensitivity is only taken into  
473 account through the selection criterion on the thermal contrast. Nonetheless following the method described in  
474 Rodgers and Connor (2003), the FTIR averaging kernel **A** is applied to the IASI profile  $x_{sat}$  to account for the  
475 effects of the a-priori information and vertical sensitivity of the FTIR retrieval (the assumed profiles, called  
476 “land” and “sea” are described in Van Damme et al., 2014a). The IASI profiles are not fully retrieved profiles  
477 but fixed shape profiles used as an assumption in the IASI retrieval, see Van Damme et al., 2015a. These fixed  
478 profiles are used for scaling purposes to be able to account for the FTIR averaging kernel. A total column

479 [averaging kernel could be used instead, but in principle is similar to the procedure described here.](#) The IASI  
 480 profile is first mapped to the altitude grid of the FTIR profile by using interpolation, forming  $x_{sat}^{mapped}$ . Applying  
 481 Eqn. (1), the smoothed IASI profile  $\hat{x}_{sat}$  is calculated indicating what the FTIR would retrieve when observing  
 482 the satellite profile, which is then used to compute a total column. This profile can then be compared with the  
 483 FTIR profile.

$$484 \hat{x}_{sat} = x_{ftir}^{priori} + A(x_{sat}^{mapped} - x_{ftir}^{priori}) \quad (1)$$

485 After the application of the averaging kernel, for each FTIR observation, all satellite observations meeting the  
 486 coincident criteria are averaged into a single mean total column value to be compared with the FTIR value. If  
 487 multiple FTIR observations match a single satellite overpass, taking into account the maximum time difference,  
 488 the FTIR observations are also averaged into a single mean total column value.

### 489 3. Results

#### 490 3.1 The influence of spatial differences between observations

491 Following the approach of Irie et al. (2012) we will first show the correlation  $r$ , the slope as well as the mean  
 492 relative difference (MRD) and the mean absolute difference (MAD) between satellite (y-axis) and FTIR NH<sub>3</sub>  
 493 total columns (x-axis) for each of the sites, as a function of the maximum allowable spatial difference between  
 494 the observations (xdiff). The relative difference (RD) is defined here as,  
 495  
 496

$$497 RD = \frac{(IASI \text{ column} - FTIR \text{ column}) \times 100}{FTIR \text{ column}} \quad (2)$$

498  
 499 A maximum relative difference of 200% was used to remove extreme outliers from the data, typically  
 500 observations under wintertime conditions. The left side of Figure 3 shows the correlation coefficients (blue  
 501 lines) and slope (red lines) for a selection of sites as a function of xdiff using a maximum allowed sampling time  
 502 difference of 90 minutes. The right side of Figure 3 shows the MRD and MAD between the satellite and FTIR  
 503 observations as a function of xdiff. The numbers on the bottom of each of the subfigures show the number of  
 504 observations used in the comparison. The values in bold beside the title of each subplot give the mean  
 505 concentrations of the IASI and FTIR observations. The bars indicate the standard deviation of the slope (left  
 506 side figures) and the relative and absolute differences (right side figures).  
 507  
 508

509 For most stations an increasing xdiff (Figure 3) means a decreasing correlation (blue lines) and a changing slope  
 510 (either decreasing or increasing with distance, red lines). This can be explained by the local character and high  
 511 variation of NH<sub>3</sub> emissions/concentration in combination with the locations of the stations. Moving further away  
 512 from a source will then generally decrease the relation between the concentration in the air and the emission  
 513 source. The same is true for satellite observations of the air concentrations, which have a large footprint  
 514 compared to the local character of a point measurement (FTIR) and the emissions. The steepness of this  
 515 decrease (or increase) tells us something about the local variation in NH<sub>3</sub> concentrations, which can be large for

516 sites near heterogeneous emission sources or in cases with low transport/turbulence and thus overall relatively  
517 low mixing.

518

519 Overall the highest correlations are seen at the Bremen site, which can partially be explained by the overall high  
520 number of observations with high concentrations (more than  $15\text{-}20 \times 10^{15}$  molecules  $\text{cm}^{-2}$ ) which generally favours  
521 the correlations. The mean column totals as well as the MRD and MAD do not change much except for the  
522 smallest xdiff criteria. The larger changes for observations within 15 km are probably due to the smaller number  
523 of observations (which follows from the relatively few IASI observations directly above or near the stations).  
524 The results show an underestimation of observed columns by IASI with the “all stations” slopes in between  
525  $\sim 0.6\text{-}0.8$ . The stations with a lower mean FTIR column totals, such as Toronto and Boulder (as well as  
526 Pasadena, Mexico City, and Lauder shown in the Appendix Figure A1) show lower correlations with most  
527 having slopes below one. The correlations decreasing with mean column totals point towards the product  
528 detection limits of the IASI- $\text{NH}_3$  product. The Toronto site has lower correlation coefficients for the smallest  
529 xdiffs, but this seems to be due to the large drop in number of observations for a xdiff of  $<15$  km. For higher  
530 xdiff criteria the correlations of the Toronto site shows results similar to Bremen. The observations at Boulder  
531 also show large differences when including more observations further away from the station. This can be  
532 explained by the land use surrounding the Boulder site. Immediately west of the measurement site is a mountain  
533 range which together with our elevation filter leads to rejection of the observations to the west. To the northeast  
534 there are some major farming areas surrounding the river banks. Correlations do increase with a decreasing  
535 xdiff, suggesting that IASI is able to resolve the large gradients in the  $\text{NH}_3$  concentrations near the site.

536

537 From the correlation analysis as function of spatial coincidence, we conclude that a xdiff value of 25 km is  
538 recommended to make a fair comparison between IASI- $\text{NH}_3$  and FTIR. Any criteria smaller than 15 km greatly  
539 reduces the number of observations and statistics. xdiff beyond 25 km further decrease the correlations for the  
540 combined set. From this point onward a xdiff value of 25 km will be used.

541

### 542 **3.2 Comparison of FTIR and IASI $\text{NH}_3$ data**

543 Observations from multiple years are used to show the coincident seasonal variability of the FTIR and IASI-  
544  $\text{NH}_3$  products for each of the sites (Figure 4, FTIR: blue, IASI: red). Observations are grouped together into a  
545 typical year as there are insufficient collocated observations to show an inter-annual time series. Note the  
546 different scales on the y-axis. Similar seasonal cycles are clearly observed in both datasets for most stations.  
547 Enhanced concentrations in spring are observed for Bremen and Toronto as well as Boulder due to manure  
548 application. Most of the sites show an increase of  $\text{NH}_3$  during the summer months which is likely due to the  
549 increased volatilization of  $\text{NH}_3$  as an effect of higher temperatures. Fire events that were earlier captured by  
550 FTIR at St.-Denis in November, as well as in the IASI data, are not observed in the collocated sets, which is due  
551 to a lack of coincident observations. Furthermore, there is a lack of observations in wintertime for most of the  
552 stations either due to low thermal contrast or due to overcast conditions. Tsukuba has observations above the  
553 detection limit but only one year of infrequent observations which is insufficient to show an entirely clear  
554 seasonal cycle. A similar thing can be said for Pasadena where the number of coincident observations are too



555 few to make meaningful conclusions about the seasonal cycle. In conclusion, IASI reflects similar pollution  
556 levels and seasonal cycles as deduced from the FTIR observations.

557

558 Figure 5 and 6 show a direct comparison of the FTIR and IASI NH<sub>3</sub> total columns for each station as well as a  
559 combination of all the observations. Correlations, number of observations and slope are shown in the figures.  
560 The MRD and these statistics are also summarized in Table 3. The comparison shows a variety of results. As  
561 before, of all 9 stations Bremen shows the best correlation with a coefficient of determination of  $r = 0.83$  and a  
562 slope of 0.60. The intercept is not fixed at zero. The stations with overall lower observed totals columns (less  
563 than  $10 \times 10^{15}$  molecules cm<sup>-2</sup>) show lower correlations. Stations with intermediate concentrations like Toronto  
564 and Boulder show correlations  $r = -0.7-0.8$ . The figure also shows the relatively low number of high  
565 observations for both the FTIR and IASI values as a result of the relatively few FTIR observations during  
566 events. The few outliers can have a disproportional effect on the slope as most of the lower observations are less  
567 accurate due to the detection limits of the instruments. Overall most stations, except St.-Denis and Boulder and  
568 Mexico City, indicate an underestimation by IASI of the FTIR columns ranging from 10-50%. The mean  
569 relative differences for most stations are negative with most showing values in between  $-22.5 \pm (54.0)$  % for  
570 Bremen down to a  $-61.3 \pm (78.7)$  % for St.-Denis. The bias shows some dependence on the total columns with  
571 the underestimation being higher at stations with high mean total columns and lower at stations with low mean  
572 total columns. An exception to this are stations with the lowest mean total columns (i.e. St.-Denis and  
573 Wollongong). The differences at St.-Denis might be explained by the fact that most IASI observations are  
574 positioned above water due to restrictions for terrain height differences. A similar thing can be said for  
575 Wollongong which is situated on the coast with hills directly to the inland. Most observations are on the border  
576 of water and land which might introduce errors in the retrieval. The combination of all observations gives a  
577 MRD of  $-32.4 \pm (56.3)$  %.

578

#### 579 **4. Discussion and conclusions**

580

581 Recent satellite products enable the global monitoring of atmospheric concentrations of NH<sub>3</sub>. Unfortunately, the  
582 validation of the satellite products of IASI (Van Damme et al., 2014a), TES (Shephard et al., 2011) and CrIS  
583 (Shephard et al., 2015a) is very limited and, so far, only based on sparse in-situ and airborne studies. Dammers et  
584 al. (2015) presented FTIR total column measurements of NH<sub>3</sub> at several places around the world and demonstrated  
585 that these data can provide information about the temporal variation of the column concentrations, which are more  
586 suitable for validation than ground-level concentrations. Ground-based remote sensing instruments have a long  
587 history for validation of satellite products. FTIR observations are already commonly used for the validation of  
588 many satellite products, including carbon monoxide (CO), methane (CH<sub>4</sub>) and nitrous oxide (N<sub>2</sub>O) (Wood et al.,  
589 2002; Griesfeller et al., 2006; Dils et al., 2006; Kerzenmacher et al., 2012). Furthermore, MAX-DOAS systems  
590 are used for the validation of retrievals for reactive gases (e.g. Irie et al., 2012), whereas AERONET is widely  
591 used to validate satellite-derived aerosol optical depth (e.g. Schaap et al., 2008). The ~~successful~~ comparison  
592 between FTIR and IASI NH<sub>3</sub> column reported here can be seen as a first step in the validation of NH<sub>3</sub> satellite  
593 products.

594

595 In this study, we collected FTIR measurements from nine locations around the world and followed the retrieval  
596 described by Dammers et al. (2015). The resulting datasets were used to quantify the bias and evaluate the  
597 seasonal variability in the IASI-NH<sub>3</sub> product. Furthermore, we assessed the collocation criteria for the satellite  
598 evaluation. Additional selection criteria based on thermal contrast, surface temperature, cloud cover and  
599 elevation differences between observations, were applied to ensure the quality of the IASI-NH<sub>3</sub> observations.  
600 The FTIR averaging kernels were applied to the satellite profiles to account for the vertical sensitivity of the  
601 FTIR and the influence of the a-priori profiles.

602  
603 To optimally compare the satellite product to the FTIR observations it is best to reduce the spatial collocation  
604 criterion to the size of the satellite instrument's footprint and allow for a time difference as short as possible.  
605 These considerations are to reduce effects of transport, chemistry and boundary layer growth but limit the  
606 number of coinciding observations significantly. We have shown that the spatial distance between the IASI  
607 observations and the FTIR measurement site is of importance: the larger the distance in space, the lower the  
608 correlation. When there is no exact match in the position of both observations the variations in the spatial  
609 separation lead to correlation coefficients that can greatly change even when changing the spatial criteria (xdiff)  
610 from 10 to 30 km. Reasons for the changes are the local nature of NH<sub>3</sub> emissions, the surrounding terrain  
611 characteristics and their influence on local transport of NH<sub>3</sub>. The small values for spatial and temporal  
612 coincidence criteria show the importance of NH<sub>3</sub> sources near the measurement sites when using these  
613 observations for satellite validation. For the validation of the IASI observations, we used a xdiff of less than 25  
614 km, which still showed high correlations while a large number of observations is retained for comparison.

615  
616 Overall we see a broad consistency between the IASI and FTIR observations. The seasonal variations of both  
617 datasets look similar for most stations. Increased column values are observed for both IASI and FTIR during  
618 summers as the result of higher temperatures, with some sites showing an increase in concentrations due to  
619 manure application and fertilization events in spring (Bremen, Toronto). In general our comparison shows that  
620 IASI underestimates the NH<sub>3</sub> total columns, except for Wollongong. The Wollongong site has persistent low  
621 background columns, i.e. observations with a low HRI, to which IASI is not very sensitive, which results in an  
622 overestimation of the observed columns. Overall, correlations range from  $r \sim 0.8$  for stations characterised by  
623 higher NH<sub>3</sub> column totals (with FTIR columns up to  $80 \times 10^{15}$  molecules cm<sup>-2</sup>) to low  $r \sim 0.4-0.5$  correlations for  
624 stations, which only have a few to no FTIR observations above  $5 \times 10^{15}$  molecules cm<sup>-2</sup>. Hence, the detection  
625 limit or sensitivity of the IASI instrument largely explain the lower correlation values. The combination of all  
626 sites ( $N_{\text{obs}} = 547$ ) give a MRD of  $-32.4 \pm (56.3) \%$ , a correlation  $r$  of 0.8 with a slope of 0.73.

627  
628 In comparison to ground-based in situ systems, the FTIR observations have the big advantage to provide coarse  
629 vertical profiles, from which a column can be derived, which are more similar to what the satellite measures and  
630 therefore more useful for validation. Dedicated NH<sub>3</sub> validation datasets are needed that better match the  
631 overpass times of satellite instruments like IASI, TES and CrIS. This could be achieved by the addition of NH<sub>3</sub>  
632 to the NDACC measurement protocols and matching the overpass time of these satellites over these  
633 measurement stations by using of the right spectral filters for detecting NH<sub>3</sub>. Furthermore, the low number of  
634 NDACC stations and their locations are not optimal for a dedicated validation of NH<sub>3</sub> satellite products.

635 Although these provide a starting point, the small set of stations does not cover the entire range of climate  
636 conditions, agricultural source types and emission regimes. Hence, our validation results should be seen as  
637 indicative. Additional stations or dedicated field campaigns are needed to improve this situation. New stations  
638 should be placed in regions where emissions and geography are homogenous to ensure that stations are  
639 representative for the footprints of the satellites. For validation of satellite products using FTIR measurements a  
640 monitoring and measurements strategy needs to be developed with a representative mixture of locations in  
641 addition to ground level data. The later can cover the spatial variation and different temporal measurements can  
642 be used. The use of IASI and FTIR observations to study NH<sub>3</sub> distributions at ground level requires a  
643 combination of model calculations and observations (e.g. Erisman et al., 2005a; 2005b). Such techniques are  
644 required to provide all the necessary details to describe the high spatial and temporal variations in NH<sub>3</sub>.

645  
646 The direct comparison of the IASI and FTIR columns is an addition to earlier efforts by Van Damme et al.  
647 (2015a) to validate IASI column observations with surface in situ and airborne observations. Our results  
648 presented here indicate that the product performs better than the previously upper bound estimate of a factor 2  
649 (i.e. -50 to +100%) as reported in Van Damme et al. (2014a). Although we tried to diminish any effect of  
650 sampling time and position it cannot be ruled out completely that these impacts the comparison statistics as the  
651 number of stations is small. Still the picture arising from the different stations is rather consistent, which hints at  
652 other issues that may explain the observed bias. A number of important issues concerning the retrieval  
653 techniques may explain the observed difference. First, the HRI based retrieval used for IASI is intrinsically  
654 different to the optimal estimation based approach used for the FTIR retrieval. An IASI optimal estimation  
655 retrieval for NH<sub>3</sub> called FORLI does exist but is not fully operationally used as it is computationally much  
656 slower than the HRI method. Surprisingly a first comparison between the FORLI and HRI based retrieval (see  
657 figure 9, Van Damme et al., 2014a) shows ~30% lower retrieved columns by the HRI scheme, which is very  
658 close to the systematic difference quantified here. Do note that the results are not be fully comparable as the  
659 reported HRI-FORLI comparison was for a limited dataset and no quality selection criteria were applied. We  
660 recommend to further explore the use of the optimal estimation based IASI-NH<sub>3</sub> retrieval in comparison to the  
661 FTIR observations. Second, the IASI and FTIR retrievals incorporate the same line spectroscopy database  
662 (HITRAN 2012; Rothman et al., 2013) which removes a possible error due to different spectroscopy datasets.  
663 The spectroscopy is the largest expected cause of error in the FTIR observations with measurement noise being  
664 the close second for sites with low concentrations. An improvement to the line parameters (i.e. line intensity,  
665 pressure and temperature effects) would greatly benefit both the FTIR and IASI retrievals. Thirdly, the HRI  
666 based scheme uses the difference between spectra with and without the spectral signature of NH<sub>3</sub>. A plausible  
667 cause for error in this scheme is the influence and correlation of interfering species in the same spectral  
668 channels. H<sub>2</sub>O lines occur near most of the NH<sub>3</sub> spectral lines and interfere with the NH<sub>3</sub> lines at the resolution  
669 of the IASI instrument. Humidity levels vary throughout the year with an increase amount of water vapour in  
670 summer conditions. The HRI based scheme uses a fixed amount of water vapour and varying amounts of water  
671 vapour may interfere with the HRI value attributed fully to the NH<sub>3</sub> columns. As there is a seasonality in the  
672 water vapour content of the atmosphere (Wagner et al., 2006), any error attributed to water vapour should show  
673 a seasonality in the difference between the IASI and FTIR observations. A seasonality was, however, not visible  
674 although it may be that the number of coincident observations was too small to recognize it. This again shows

675 the need for dedicated NH<sub>3</sub> validation data (e.a. dedicated FTIR observations). Fourth, the negative bias of the  
676 satellite observations can be expected by the lack of sensitivity to concentrations near the surface. This is of  
677 course where the ammonia concentrations usually peak. The FTIR observations however do fully observe the  
678 lower layers in the troposphere thus causing a discrepancy. Normally one can correct for this using the  
679 averaging kernel of the satellite observations. However, the IASI-NH<sub>3</sub> retrieval does not produce an averaging  
680 kernel meaning it is not possible to calculate the exact effect. The use of a typical averaging kernel will cause  
681 more uncertainty as there is a large day to day variability in the averaging kernels as earlier retrievals showed  
682 (Clarisse et al., 2009). Finally, another possible cause of error is the lack of a varying NH<sub>3</sub> profile and the proxy  
683 used for thermal contrast to describe the state of the atmosphere. The sensitivity of the scheme to the  
684 concentrations of NH<sub>3</sub> in the boundary layer is described by using a fixed profile for land and sea observations  
685 in combination with a thermal contrast based on two layers (surface and 1.5 km) as it is expected that most of  
686 the NH<sub>3</sub> occurs in the boundary layer. In reality the NH<sub>3</sub> profile is highly dynamic due to a varying boundary  
687 layer height and changing emissions as well as temperature changes (e.g. inversions etc) occurring throughout  
688 the planetary boundary layer. Not accounting for this can introduce an error and future HRI based schemes  
689 should focus on estimating the possible effects of using only a specific profile. The use of multiple NH<sub>3</sub>-profiles  
690 in combination with multiple temperature layers would be a better approximation of state of the atmosphere,  
691 although computationally more expensive. The sharp difference between the sea and land retrieval introduces  
692 strong variability in observations near the coast. Furthermore, observations that are directly on the transition  
693 between water and land can introduce problems due to the varying emissivity. Similar issues have been reported  
694 for aerosol retrievals (e.g. Schaap et al., 2008).

695 Although the FTIR observations offer some vertical information, studies combining this technique with tower or  
696 airborne observations are needed to further improve knowledge and sensitivity of the FTIR and satellite  
697 observations to the vertical distribution of NH<sub>3</sub>. Without this knowledge, it is not possible to use the  
698 observations for quantitative emission estimates and modelling purposes as no uncertainty on the new estimate  
699 can be given. Approaches similar to the recent study by Shepherd-Shephard et al. (2015b) using an airborne  
700 instrument, possibly in combination with an FTIR system focused on the overpass of multiple satellite systems  
701 for an extended period of time should be used to establish the sensitivities and biases of the different retrieval  
702 products available from satellite instruments as well as the bias between the satellite and surface instruments.  
703 The use of IASI and FTIR observations to study NH<sub>3</sub> distributions at ground level requires a combination of  
704 model calculations and observations. Such techniques are required to provide all the necessary details to  
705 describe the high spatial and temporal variations in NH<sub>3</sub>.

#### 707 **Acknowledgements**

709 This work is part of the research programme GO/12-36, which is financed by the Netherlands Organisation for  
710 Scientific Research (NWO). The Lauder NIWA FTIR program is funded through the New Zealand  
711 government's core research grant framework from the Ministry of Business, Innovation and employment. We  
712 thank the Lauder FTIR team for their contribution. Acknowledgements are addressed to the Université de La  
713 Réunion and CNRS (LACy-UMR8105 and UMS3365) for their support of the Reunion Island measurements.  
714 The Reunion Island data analysis has mainly been supported by the A3C project (PRODEX Program of the

Formatted: Subscript

715 Belgian Science Policy Office, BELSPO, Brussels). The University of Toronto's NDACC contribution has been  
716 supported by the CAFTON project, funded by the Canadian Space Agency's FAST Program. Measurements  
717 were made at the University of Toronto Atmospheric Observatory (TAO), which has been supported by  
718 CFCAS, ABB Bomem, CFI, CSA, EC, NSERC, ORDCF, PREA, and the University of Toronto. Part of this  
719 research was performed at the Jet Propulsion Laboratory, California Institute of Technology, under contract with  
720 NASA. IASI has been developed and built under the responsibility of the "Centre national d'études spatiales"  
721 (CNES, France). It is flown on-board the Metop satellites as part of the EUMETSAT Polar System. The IASI  
722 L1 data are received through the EUMETCast near real-time data distribution service.  
723 The IASI-related activities in Belgium were funded by Belgian Science Policy Office through the IASI.Flow  
724 Prodex arrangement (2014-2018). PFC, LC and MVD also thank the FRS-FNRS for financial support. L.C. is a  
725 research associate with the Belgian F.R.S-FNRS. C. Clerbaux is grateful to CNES for scientific collaboration  
726 and financial support. The National Center for Atmospheric Research is supported by the National Science  
727 Foundation. The Boulder observation program is supported in part by the Atmospheric Chemistry Observations  
728 & Modeling Division of NCAR. The measurement programme and NDACC site at Wollongong has been  
729 supported by the Australian Research Council for many years, most recent by grant DP110101948 and  
730 LE0668470. The Mexico City site was funded through projects UNAM-DGAPA (109914) and CONACYT  
731 (249374, 239618). A. Bezanilla, J. Baylón and E. Plaza are acknowledged for their participation in the  
732 measurements and analysis. We would like to thank David Griffith, Clare Murphy and Voltaire Velazco at the  
733 School of Chemistry, University of Wollongong, for maintaining FTS instrumentation and conducting FTS  
734 measurements. We are grateful to the many colleagues who have contributed to FTIR data acquisition at the  
735 various sites.

736

737 **References**

- 738  
739 Adams, P.J., Seinfeld, J.H., Koch, D., Mickley, L., Jacob, D. (2001), General circulation model assessment of  
740 direct radiative forcing by the sulfate-nitrate-ammonium-water inorganic aerosol system, *Journal of Geophysical*  
741 *Research Atmospheres*, 106 (1), pp. 1097-1111.
- 742  
743 [August, T., Klaes, D., Schlüssel, P., Hultberg, T., Crapeau, M., Arriaga, A., O'Carroll, A., Coppens, D., Munro,](#)  
744 [R. and Calbet, X.: IASI on Metop-A: Operational Level 2 retrievals after five years in orbit, \*J. Quant. Spectrosc.\*](#)  
745 [Radiat. Transf., 113\(11\), 1340–1371, doi:10.1016/j.jqsrt.2012.02.028, 2012.](#)
- 746  
747 Beer, R., Shephard, M. W., Kulawik, S. S., Clough, S. a., Eldering, A., Bowman, K. W., Sander, S. P., Fisher, B.  
748 M., Payne, V. H., Luo, M., Osterman, G. B. and Worden, J. R.: First satellite observations of lower tropospheric  
749 ammonia and methanol, *Geophys. Res. Lett.*, 35(9), 1–5, doi:10.1029/2008GL033642, 2008.
- 750  
751 Bleeker, A., Sutton, M. A., Acherman, B., Alebic-Juretic, A., Aneja, V. P., Ellermann, T., Erisman, J. W., Fowler,  
752 D., Fagerli, H., Gauger, T., Harlen, K. S., Hole, L. R., Horvath, L., Mitisinkova, M., Smith, R. I., Tang, Y. S.,  
753 and Pul, A.: Linking ammonia emission trends to measured concentrations and deposition of reduced nitrogen at  
754 different scales, in: *Atmospheric Ammonia – Detecting emission changes and environmental impacts. Results of*  
755 *an expert workshop under the convention of long-range transboundary air pollution*, edited by: Sutton M. A., Reis  
756 S., Baker S. M. H. , *Atmospheric Ammonia – Detecting emission changes and environmental impacts. Results of*  
757 *an expert workshop under the convention of long-range transboundary air pollution*, Springer, 123–180, 2009.
- 758  
759 Bobbink, R, Hicks K, Galloway J, Spranger T, Alkemade R, Ashmore M, Bustamante M, Cinderby S, Davidson  
760 E, Dentener F, Emmett B, Erisman JW, Fenn M, Gilliam F, Nordin A, Pardo L, De Vries W. Global assessment  
761 of nitrogen deposition effects on terrestrial plant diversity: a synthesis, *Ecological Applications*, 20 (2010), pp.  
762 30–59.
- 763  
764 von Bobrutzki, K., Braban, C. F., Famulari, D., Jones, S. K., Blackall, T., Smith, T. E. L., Blom, M., Coe, H.,  
765 Gallagher, M., Ghalaieny, M., McGillen, M. R., Percival, C. J., Whitehead, J. D., Ellis, R., Murphy, J.,  
766 Mohacsi, A., Pogany, A., Junninen, H., Rantanen, S., Sutton, M. A., and Nemitz, E.: Field inter-comparison of  
767 eleven atmospheric ammonia measurement techniques, *Atmos. Meas. Tech.*, 3, 91-112, doi:10.5194/amt-3-91-  
768 2010, 2010.
- 769  
770 Brown, L. R., M. R. Gunson, R. A. Toth, F. W. Irion, C. P. Rinsland, and A. Goldman. "1995 atmospheric trace  
molecule spectroscopy (ATMOS) linelist." *Applied optics* 35, no. 16 (1996): 2828-2848.
- 771  
772 Chang, L., Palo, S., Hagan, M., Richter, J., Garcia, R., Riggin, D. and Fritts, D.: Structure of the migrating diurnal  
773 tide in the Whole Atmosphere Community Climate Model (WACCM), *Advances in Space Research*, 41(9), 1398–  
1407, doi:10.1016/j.asr.2007.03.035, 2008.
- 774  
775 Coheur, P.-F., Clarisse, L., Turquety, S., Hurtmans, D., and Clerbaux, C.: IASI measurements of reactive trace  
species in biomass burning plumes, *Atmos. Chem. Phys.*, 9, 5655-5667, doi:10.5194/acp-9-5655-2009, 2009.
- 776  
777 Clarisse, Lieven, Cathy Clerbaux, Frank Dentener, Daniel Hurtmans, and Pierre-François Coheur. "Global  
ammonia distribution derived from infrared satellite observations." *Nature Geoscience* 2, no. 7 (2009): 479-483.
- 778  
779 Clarisse, L., Shephard, M. W., Dentener, F., Hurtmans, D., Cady-Pereira, K., Karagulian, F., Van Damme, M.,  
Clerbaux, C. and Coheur, P.-F.: Satellite monitoring of ammonia: A case study of the San Joaquin Valley, *J.*  
780 *Geophys. Res.*, 115(D13), 1–15, doi:10.1029/2009JD013291, 2010.
- 781  
782 Dammers, E., Vigouroux, C., Palm, M., Mahieu, E., Warneke, T., Smale, D., Langerock, B., Franco, B., Van  
783 Damme, M., Schaap, M., Notholt, J., and Erisman, J. W.: Retrieval of ammonia from ground-based FTIR solar  
spectra, *Atmos. Chem. Phys.*, 15, 12789-12803, doi:10.5194/acp-15-12789-2015, 2015.
- 784  
785 Dentener, F. J. and Crutzen, P. J.: A three-dimensional model of the global ammonia cycle, *J. Atmos. Chem.*,  
19(4), 331–369, doi:10.1007/BF00694492, 1994.
- 786  
787 Dentener, F., Drevet, J., Lamarque, J. F., Bey, I., Eickhout, B., Fiore, A. M., Hauglustaine, D., Horowitz, L. W.,  
Krol, M., Kulshrestha, U. C., Lawrence, M., Galy-Lacaux, C., Rast, S., Shindell, D., Stevenson, D., Van Noije,  
788 T., Atherton, C., Bell, N., Bergman, D., Butler, T., Cofala, J., Collins, B., Doherty, R., Ellingsen, K., Galloway,  
789 J., Gauss, M., Montanaro, V., Müller, J. F., Pitari, G., Rodriguez, J., Sanderson, M., Solmon, F., Strahan, S.,

790 Schultz, M., Sudo, K., Szopa, S. and Wild, O.: Nitrogen and sulfur deposition on regional and global scales: A  
791 multimodel evaluation, *Global Biogeochem. Cycles*, 20(4), doi:10.1029/2005GB002672, 2006.  
792  
793  
794 Dils, B., De Mazière, M., Müller, J. F., Blumenstock, T., Buchwitz, M., de Beek, R., Demoulin, P., Duchatelet, P.,  
795 Fast, H., Frankenberg, C., Gloudemans, A., Griffith, D., Jones, N., Kerzenmacher, T., Kramer, I., Mahieu, E.,  
796 Mellqvist, J., Mittermeier, R. L., Notholt, J., Rinsland, C. P., Schrijver, H., Smale, D., Strandberg, A.,  
797 Straume, A. G., Stremme, W., Strong, K., Sussmann, R., Taylor, J., van den Broek, M., Velasco, V., Wagner, T.,  
798 Warneke, T., Wiacek, A., and Wood, S.: Comparisons between SCIAMACHY and ground-based FTIR data for  
799 total columns of CO, CH<sub>4</sub>, CO<sub>2</sub> and N<sub>2</sub>O, *Atmos. Chem. Phys.*, 6, 1953-1976, doi:10.5194/acp-6-1953-2006,  
800 2006.

801 EDGAR-Emission Database for Global Atmospheric Research: Source: EC-JRC/PBL. EDGAR version 4.2.,  
802 <http://edgar.jrc.ec.europa.eu>, access 15th October 2012, 2011  
803

804 Erisman, J. W., Hensen, A., Mosquera, J., Sutton, M. and Fowler, D.: Deposition monitoring networks: what  
805 monitoring is required to give reasonable estimates of ammonia/ammonium?, *Environ. Pollut.*, 135(3), 419–431,  
806 doi:<http://dx.doi.org/10.1016/j.envpol.2004.11.015>, 2005a.  
807

808 Erisman, J. W., Vermeulen, A., Hensen, A., Flechard, C., Dämmgen, U., Fowler, D., Sutton, M., Grünhage, L.  
809 and Tuovinen, J. P.: Monitoring and modelling of biosphere/atmosphere exchange of gases and aerosols in  
810 Europe, *Environ. Pollut.*, 133(3), 403–413, doi:10.1016/j.envpol.2004.07.004, 2005b.  
811

812 Erisman, J. W., Bleeker, a., Galloway, J. and Sutton, M. S.: Reduced nitrogen in ecology and the environment,  
813 *Environ. Pollut.*, 150(1), 140–149, doi:10.1016/j.envpol.2007.06.033, 2007.  
814

815 Erisman, J. W., Sutton, M. a., Galloway, J., Klimont, Z. and Winiwarter, W.: How a century of ammonia synthesis  
816 changed the world, , 1(October 1908), doi:10.1038/ngeo325, 2008.  
817

818 Erisman, J. W., Galloway, J., Seitzinger, S., Bleeker, A. and Butterbach-Bahl, K.: Reactive nitrogen in the  
819 environment and its effect on climate change, *Curr. Opin. Environ. Sustain.*, 3(5), 281–290,  
820 doi:10.1016/j.cosust.2011.08.012, 2011.  
821

822 Farr, T. G., Rosen, P. a., Caro, E. and Crippen, R.: The Shuttle Radar Topography Mission, *Rev. ....*, (2005), 1–  
823 33, doi:10.1029/2005RG000183.1.INTRODUCTION, 2007.  
824

825 Fowler, D., Coyle, M., Skiba, U., Sutton, M. A., Cape, J. N., Reis, S., Sheppard, L. J., Jenkins, A., Grizzetti, B.,  
826 Galloway, J. N., Vitousek, P., Leach, A., Bouwman, A. F., Butterbach-Bahl, K., Dentener, F., Stevenson, D.,  
827 Amann, M. and Voss, M.: The global nitrogen cycle in the twenty-first century, *Philos. Trans. R. Soc. London B*  
828 *Biol. Sci.*, 368(1621) [online] Available from:  
829 <http://rstb.royalsocietypublishing.org/content/368/1621/20130164.abstract>, 2013.  
830

831 Griesfeller, a., Griesfeller, J., Hase, F., Kramer, I., Loës, P., Mikuteit, S., Raffalski, U., Blumenstock, T. and  
832 Nakajima, H.: Comparison of ILAS-II and ground-based FTIR measurements of O<sub>3</sub>, HNO<sub>3</sub>, N<sub>2</sub>O, and CH<sub>4</sub>  
833 over Kiruna, Sweden, *J. Geophys. Res.*, 111(D11), D11S07, doi:10.1029/2005JD006451, 2006.  
834

835 Hase, F., Blumenstock, T. and Paton-Walsh, C.: Analysis of the instrumental line shape of high-resolution  
836 fourier transform IR spectrometers with gas cell measurements and new retrieval software., *Appl. Opt.*, 38(15),  
837 3417–3422, 1999.  
838

839 Hase, F., Hannigan, J. W., Coffey, M. T., Goldman, a., Höpfner, M., Jones, N. B., Rinsland, C. P. and Wood, S.  
840 W.: Intercomparison of retrieval codes used for the analysis of high-resolution, ground-based FTIR  
841 measurements, *J. Quant. Spectrosc. Radiat. Transf.*, 87(1), 25–52, doi:10.1016/j.jqsrt.2003.12.008, 2004.  
842

843 Hase, F., Demoulin, P., Sauval, A. J., Toon, G. C., Bernath, P. F., Goldman, A., Hannigan, J. W., Rinsland, C. P.:  
844 An empirical line-by-line model for the infrared solar transmittance spectrum from 700 to 5000 cm<sup>-1</sup>, *J. Quant.*  
845 *Spectrosc. Ra.*, 102, 450–463, doi:10.1016/j.jqsrt.2006.02.026, 2006.  
846

847 Holland, E. a., Dentener, F. J., Braswell, B. H. and Sulzman, J. M.: Contemporary and pre-industrial global  
848 reactive nitrogen budgets, *Biogeochemistry*, 46(1-3), 7–43, doi:10.1007/BF01007572, 1999.

849  
850 Irie, H., Boersma, K. F., Kanaya, Y., Takashima, H., Pan, X. and Wang, Z. F.: Quantitative bias estimates for  
851 tropospheric NO<sub>2</sub> columns retrieved from SCIAMACHY, OMI, and GOME-2 using a common standard for  
852 East Asia, *Atmos. Meas. Tech.*, 5(10), 2403–2411, doi:10.5194/amt-5-2403-2012, 2012.  
853  
854 Kerzenmacher, T., Dils, B., Kumps, N., Blumenstock, T., Clerbaux, C., Coheur, P.-F., Demoulin, P., García, O.,  
855 George, M., Griffith, D. W. T., Hase, F., Hadji-Lazaro, J., Hurtmans, D., Jones, N., Mahieu, E., Notholt, J., Paton-  
856 Walsh, C., Raffalski, U., Ridder, T., Schneider, M., Servais, C., and De Mazière, M.: Validation of IASI FORLI  
857 carbon monoxide retrievals using FTIR data from NDACC, *Atmos. Meas. Tech.*, 5, 2751–2761, doi:10.5194/amt-  
858 5-2751-2012, 2012.  
859  
860  
861 Leen, J. B., Yu, X. Y., Gupta, M., Baer, D. S., Hubbe, J. M., Kluzek, C. D., Tomlinson, J. M. and Hubbell, M. R.:  
862 Fast in situ airborne measurement of ammonia using a mid-infrared off-axis ICOS spectrometer, *Environ. Sci.*  
863 *Technol.*, 47(18), 10446–10453, doi:10.1021/es401134u, 2013.  
864  
865 Luo, M., Shephard, M. W., Cady-Pereira, K. E., Henze, D. K., Zhu, L., Bash, J. O., Pinder, R. W., Capps, S. L.,  
866 Walker, J. T. and Jones, M. R.: Satellite observations of tropospheric ammonia and carbon monoxide: Global  
867 distributions, regional correlations and comparisons to model simulations, *Atmos. Environ.*, 106, 262–277,  
868 doi:10.1016/j.atmosenv.2015.02.007, 2015.  
869  
870 Lutsch, E., Dammers, E., Conway, S. and Strong, K.: Ground-based FTIR measurements of CO, HCN, C<sub>2</sub>H<sub>6</sub> and  
871 NH<sub>3</sub> emissions from the 2014 Canadian Wildfires, *in preparation*.  
872  
873 Morgenstern, O., Zeng, G., Wood, S. W., Robinson, J., Smale, D., Paton-Walsh, C., Jones, N. B., and Griffith,  
874 D. W. T.: Long-range correlations in Fourier transform infrared, satellite, and modeled CO in the Southern  
875 Hemisphere, *J. Geophys. Res.*, 117, D11301 doi:10.1029/2012JD017639, 2012.  
876  
877 Moya, M., Fountoukis, C., Nenes, A., Matías, E., and Grutter, M.: Predicting diurnal variability of fine  
878 inorganic aerosols and their gas-phase precursors near downtown Mexico City, *Atmos. Chem. Phys. Discuss.*, 7,  
879 11257–11294, doi:10.5194/acpd-7-11257-2007, 2007.  
880  
881 Nowak, J. B., Neuman, J. A., Kozai, K., Huey, L. G., Tanner, D. J., Holloway, J. S., Ryerson, T. B., Frost, G. J.,  
882 McKeen, S. A., and Fehsenfeld, F. C.: A chemical ionization mass spectrometry technique for airborne  
883 measurements of ammonia, *J. Geophys. Res.-Atmos.*, 112, D10S02, doi:10.1029/2006JD007589, 2007.  
884  
885 Nowak, J. B., Neuman, J. A., Bahreini, R., Brock, C. A., Middlebrook, A. M., Wollny, A. G., Holloway, J. S.,  
886 Peischl, J., Ryerson, T. B., and Fehsenfeld, F. C.: Airborne observations of ammonia and ammonium nitrate  
887 formation over Houston, Texas, *J. Geophys. Res.-Atmos.*, 115, D22 304, doi:10.1029/2010JD014195, 2010.  
888  
889 Ohshima, H., Morino, I., Nagahama, T., Machida, T., Suto, H., Oguma, H., Sawa, Y., Matsueda, H., Sugimoto,  
890 N., Nakane, H., and Nakagawa, K.: Column-averaged volume mixing ratio of CO<sub>2</sub> measured with ground-based  
891 Fourier transform spectrometer at Tsukuba, *J. Geophys. Res.*, 114, D18303, doi:10.1029/2008JD011465, 2009.  
892  
893 Paton-Walsh, C., Jones, N. B., Wilson, S. R., Haverd, V., Meier, A., Griffith, D. W. T. and Rinsland, C. P.  
894 (2005), Measurements of trace gas emissions from Australian forest fires and correlations with coincident  
895 measurements of aerosol optical depth, *J. Geophys. Res.*, 110, D24305, doi:10.1029/2005JD006202  
896  
897 Pope, III, C. A., Ezzati, M., and Dockery, D. W.: Fine-Particulate Air Pollution and Life Expectancy in the United  
898 States, *N. Engl. J. Med.*, 360, 376–386, doi:10.1056/NEJMsa0805646, 2009.  
899  
900 Pougatchev, N. S., Connor, B. J., & Rinsland, C. P. (1995). Infrared measurements of the ozone vertical  
901 distribution above Kitt Peak. *Journal of Geophysical Research: Atmospheres (1984–2012)*, 100(D8), 16689-  
902 16697.  
903  
904 Puchalski, M. A., M. E. Sather, J. T. Walker, C. M. Lehmann, D. A. Gay, J. Mathew, and W. P. Robarge (2011),  
905 Passive ammonia monitoring in the United States: Comparing three different sampling devices, *J. Environ. Monit.*,  
906 13(11), 3156–3167, doi:10.1039/c1em10553a.  
907



908 Ravishankara, A. R., Daniel, J. S. and Portmann, R. W.: Nitrous oxide (N<sub>2</sub>O): the dominant ozone-depleting  
909 substance emitted in the 21st century., *Science*, 326(5949), 123–125, doi:10.1126/science.1176985, 2009.  
910

911 Rockstrom, J., Steffen, W., Noone, K., Persson, A., Chapin, F. S., Lambin, E. F., Lenton, T. M., Scheffer, M.,  
912 Folke, C., Schellnhuber, H. J., Nykvist, B., de Wit, C. A., Hughes, T., van der Leeuw, S., Rodhe, H., Sorlin, S.,  
913 Snyder, P. K., Costanza, R., Svedin, U., Falkenmark, M., Karlberg, L., Corell, R. W., Fabry, V. J., Hansen, J.,  
914 Walker, B., Liverman, D., Richardson, K., Crutzen, P. and Foley, J. A.: A safe operating space for humanity,  
915 *Nature*, 461(7263), 472–475 [online] Available from: <http://dx.doi.org/10.1038/461472a>, 2009.  
916

917 Rodgers, C. D.: *Inverse Methods for Atmospheric Sounding - Theory and Practice*, 2(January), 256,  
918 doi:10.1142/9789812813718, 2000.  
919

920 Rodgers, C. D. and Connor, B. J.: Intercomparison of remote sounding instruments, *J. Geophys. Res. Atmos.*,  
921 108(D3), n/a–n/a, doi:10.1029/2002JD002299, 2003.  
922

923 Rodhe, Henning, Frank Dentener, and Michael Schulz. "The global distribution of acidifying wet  
924 deposition." *Environmental Science & Technology* 36.20 (2002): 4382-4388.  
925

926 Rothman, L. S., Gordon, I. E., Babikov, Y., Barbe, a., Chris Benner, D., Bernath, P. F., Birk, M., Bizzocchi, L.,  
927 Boudon, V., Brown, L. R., Campargue, a., Chance, K., Cohen, E. a., Coudert, L. H., Devi, V. M., Drouin, B. J.,  
928 Fayt, a., Flaud, J. M., Gamache, R. R., Harrison, J. J., Hartmann, J. M., Hill, C., Hodges, J. T., Jacquemart, D.,  
929 Jolly, a., Lamouroux, J., Le Roy, R. J., Li, G., Long, D. a., Lyulin, O. M., Mackie, C. J., Massie, S. T.,  
930 Mikhailenko, S., Müller, H. S. P., Naumenko, O. V., Nikitin, a. V., Orphal, J., Perevalov, V., Perrin, a.,  
931 Polovtseva, E. R., Richard, C., Smith, M. a H., Starikova, E., Sung, K., Tashkun, S., Tennyson, J., Toon, G. C.,  
932 Tyuterev, V. G. and Wagner, G.: The HITRAN2012 molecular spectroscopic database, *J. Quant. Spectrosc.*  
933 *Radiat. Transf.*, 130, 4–50, doi:10.1016/j.jqsrt.2013.07.002, 2013.  
934

935 Schaap, M., van Loon, M., ten Brink, H. M., Dentener, F. J., and Builtjes, P. J. H.: Secondary inorganic aerosol  
936 simulations for Europe with special attention to nitrate, *Atmos. Chem. Phys.*, 4, 857-874, doi:10.5194/acp-4-857-  
937 2004, 2004  
938

939 Schaap, M., Timmermans, R. M. a, Koelemeijer, R. B. a, de Leeuw, G. and Builtjes, P. J. H.: Evaluation of  
940 MODIS aerosol optical thickness over Europe using sun photometer observations, *Atmos. Environ.*, 42(9), 2187–  
941 2197, doi:10.1016/j.atmosenv.2007.11.044, 2008.  
942

943 Senten, C., De Mazière, M., Dils, B., Hermans, C., Kruglanski, M., Neefs, E., Scolas, F., Vandaele, A. C.,  
944 Vanhaelewyn, G., Vigouroux, C., Carleer, M., Coheur, P. F., Fally, S., Barret, B., Baray, J. L., Delmas, R., Leveau,  
945 J., Metzger, J. M., Mahieu, E., Boone, C., Walker, K. A., Bernath, P. F., and Strong, K.: Technical Note: New  
946 ground-based FTIR measurements at Ile de La Réunion: observations, error analysis, and comparisons with  
947 independent data, *Atmos. Chem. Phys.*, 8, 3483-3508, doi:10.5194/acp-8-3483-2008, 2008.  
948

949 Shephard, M. W., Cady-Pereira, K. E., Luo, M., Henze, D. K., Pinder, R. W., Walker, J. T., Rinsland, C. P.,  
950 Bash, J. O., Zhu, L., Payne, V. H., and Clarisse, L.: TES ammonia retrieval strategy and global observations of  
951 the spatial and seasonal variability of ammonia, *Atmos. Chem. Phys.*, 11, 10743-10763, doi:10.5194/acp-11-  
952 10743-2011, 2011.

953 Shephard, M. W. and Cady-Pereira, K. E.: Cross-track Infrared Sounder (CrIS) satellite observations of  
954 tropospheric ammonia, *Atmos. Meas. Tech.*, 8, 1323-1336, doi:10.5194/amt-8-1323-2015, 2015a.

955 Shephard, M. W., McLinden, C. A., Cady-Pereira, K. E., Luo, M., Moussa, S. G., Leithead, A., Liggio, J., Staebler,  
956 R. M., Akingunola, A., Makar, P., Lehr, P., Zhang, J., Henze, D. K., Millet, D. B., Bash, J. O., Zhu, L., Wells, K.  
957 C., Capps, S. L., Chaliyakunnel, S., Gordon, M., Hayden, K., Brook, J. R., Wolde, M., and Li, S.-M.: Tropospheric  
958 Emission Spectrometer (TES) satellite validations of ammonia, methanol, formic acid, and carbon monoxide over  
959 the Canadian oil sands, *Atmos. Meas. Tech. Discuss.*, 8, 9503-9563, doi:10.5194/amt-d-8-9503-2015, 2015b.

960 Slanina, J., ten Brink, H. M., Otjes, R. P., Even, A., Jongejan, P., Khlystov, A., Waijers-Ijpelaan, A., Hu, M., and  
961 Lu, Y.: Continuous analysis of nitrate and ammonium in aerosols by the Steam Jet Aerosol Collector (SJAC),  
962 *Atmos. Environ.*, 35, 2319–2330, 2001.

963 Stremme, W., Ortega, I., and Grutter, M.: Using ground-based solar and lunar infrared spectroscopy to study the  
964 diurnal trend of carbon monoxide in the Mexico City boundary layer, *Atmos. Chem. Phys.*, 9, 8061-8078,  
965 doi:10.5194/acp-9-8061-2009, 2009.

966 Stremme, W., Grutter, M., Rivera, C., Bezanilla, A., Garcia, A. R., Ortega, I., George, M., Clerbaux, C., Coheur,  
967 P.-F., Hurtmans, D., Hannigan, J. W., and Coffey, M. T.: Top-down estimation of carbon monoxide emissions  
968 from the Mexico Megacity based on FTIR measurements from ground and space, *Atmos. Chem. Phys.*, 13, 1357-  
969 1376, doi:10.5194/acp-13-1357-2013, 2013.

970 Sutton, M., Stefan Reis, and Samantha MH Baker. "Atmospheric ammonia." *Detecting Emission Changes and*  
971 *Environmental Impacts* 494 (2009).

972 Sutton, M. a, Reis, S., Riddick, S. N., Dragosits, U., Nemitz, E., Theobald, M. R., Tang, Y. S., Braban, C. F.,  
973 Vieno, M., Dore, A. J., Mitchell, R. F., Wanless, S., Daunt, F., Fowler, D., Blackall, T. D., Milford, C., Flechard,  
974 C. R., Loubet, B., Massad, R., Cellier, P., Personne, E., Coheur, P. F., Clarisse, L., Van Damme, M., Ngadi, Y.,  
975 Clerbaux, C., Skj oth, C. A., Geels, C., Hertel, O., Wichink Kruit, R. J., Pinder, R. W., Bash, J. O., Walker, J. T.,  
976 Simpson, D., Horv ath, L., Misselbrook, T. H., Bleeker, A., Dentener, F. and de Vries, W.: Towards a climate-  
977 dependent paradigm of ammonia emission and deposition., *Philos. Trans. R. Soc. Lond. B. Biol. Sci.*, 368(1621),  
978 20130166, doi:10.1098/rstb.2013.0166, 2013.

979 Sun, K., Cady-Pereira, K., Miller, D. J. , Tao, L., Zondlo, M.A. , Nowak, J. B., Neuman, J. A., Mikoviny, T.,  
980 M uller, M. ,Wisthaler, A., Scarino, A. J., and Hostetler, C. A.: Validation of TES ammonia observations at the  
981 single pixel scale in theSan Joaquin Valley during DISCOVER-AQ, *J. Geophys. Res.-Atmos.*, 120, 5140–5154,  
982 doi:10.1002/2014JD022846, 2015.

983  
984 Toon, G. C., Blavier, J.-F., Sen, B., Margitan, J. J., Webster, C. R., Max, R. D., Fahey, D. W., Gao, R., DelNegro,  
985 L., Proffitt, M., Elkins, J., Romashkin, P. A., Hurst, D. F., Oltmans, S., Atlas, E., Schauffler, S., Flocke, F., Bui,  
986 T. P., Stimpfle, R. M., Bonne, G. P., Voss, P. B., and Cohen, R. C.: Comparison of MkIV balloon and ER-2  
987 aircraft measurements of atmospheric trace gases, *J. Geophys. Res.*, 104, 26 779–26 790, 1999.

988  
989 Van Damme, M., Clarisse, L., Heald, C. L., Hurtmans, D., Ngadi, Y., Clerbaux, C., Dolman, A. J., Erisman, J. W.,  
990 and Coheur, P. F.: Global distributions, time series and error characterization of atmospheric ammonia (NH<sub>3</sub>) from  
991 IASI satellite observations, *Atmos. Chem. Phys.*, 14, 2905-2922, doi:10.5194/acp-14-2905-2014, 2014a.

992  
993 Van Damme, M., R. J. Wichink Kruit, M. Schaap, L. Clarisse, C. Clerbaux, P.-F. Coheur, E. Dammers, A. J.  
994 Dolman, and J. W. Erisman , Evaluating 4 years of atmospheric ammonia (NH<sub>3</sub>) over Europe using IASI satellite  
995 observations and LOTOS-EUROS model results, *J. Geophys. Res. Atmos.*, 119, 9549–9566,  
996 doi:10.1002/2014JD021911, 2014b.

997  
998 Van Damme, M., Clarisse, L., Dammers, E., Liu, X., Nowak, J. B., Clerbaux, C., Flechard, C. R., Galy-Lacaux,  
999 C., Xu, W., Neuman, J. a., Tang, Y. S., Sutton, M. a., Erisman, J. W. and Coheur, P. F.: Towards validation of  
1000 ammonia (NH<sub>3</sub>) measurements from the IASI satellite, *Atmos. Meas. Tech.*, 8(3), 1575–1591, doi:10.5194/amt-  
1001 8-1575-2015, 2015a.

1002  
1003 Van Damme, M., J. W. Erisman, L. Clarisse, E. Dammers, S. Whitburn, C. Clerbaux, A. J. Dolman, and P.-F.  
1004 Coheur (2015b), Worldwide spatiotemporal atmospheric ammonia (NH<sub>3</sub>) columns variability revealed by  
1005 satellite, *Geophys. Res. Lett.*, 42, doi:10.1002/2015GL065496.

1006  
1007 Velazco, V., Wood, S. W., Sinnhuber, M., Kramer, I., Jones, N. B., Kasai, Y., Notholt, J., Warneke, T.,  
1008 Blumenstock, T., Hase, F., Murcray, F. J., and Schrems, O.: Annual variation of strato-mesospheric carbon  
1009 monoxide measured by ground-based Fourier transform infrared spectrometry, *Atmos. Chem. Phys.*, 7, 1305-  
1010 1312, doi:10.5194/acp-7-1305-2007, 2007.

1011  
1012 Vigouroux, C., Hendrick, F., Stavrakou, T., Dils, B., De Smedt, I., Hermans, C., Merlaud, A., Scolas, F., Senten,  
1013 C., Vanhaelewyn, G., Fally, S., Carleer, M., Metzger, J.-M., M uller, J.-F., Van Roozendael, M., and De  
1014 Mazi ere, M.: Ground-based FTIR and MAX-DOAS observations of formaldehyde at R union Island and  
1015 comparisons with satellite and model data, *Atmos. Chem. Phys.*, 9, 9523-9544, doi:10.5194/acp-9-9523-2009,  
1016 2009.

1017

1018 Wagner, T., Beirle, S., Grzegorski, M. and Platt, U.: Global trends (1996-2003) of total column precipitable  
1019 water observed by Global Ozone Monitoring Experiment (GOME) on ERS-2 and their relation to near-surface  
1020 temperature, *J. Geophys. Res. Atmos.*, 111(12), 1–15, doi:10.1029/2005JD006523, 2006.  
1021  
1022 Whitburn, S., Van Damme, M., Kaiser, J. W., van der Werf, G. R., Turquety, S., Hurtmans, D., Clarisse, L.,  
1023 Clerbaux, C. and Coheur, P.-F.: Ammonia emissions in tropical biomass burning regions: Comparison between  
1024 satellite-derived emissions and bottom-up fire inventories, *Atmos. Environ.*, 1–13,  
1025 doi:10.1016/j.atmosenv.2015.03.015, 2015.  
1026  
1027 Whitburn, S. Van Damme, M., Clarisse, L., Heald, C., Bauduin, S., Hadji-Lazaro, J., Hurtmans, D., Clerbaux,  
1028 C. and Coheur P.-F.: A flexible and robust IASI-NH 3 retrieval algorithm, 2015 (in preparation)  
1029  
1030 Wiacek, A., Taylor, J. R., Strong, K., Saari, R., Kerzenmacher, T. E., Jones, N. B. and Griffith, D. W. T.:  
1031 Ground-Based Solar Absorption FTIR Spectroscopy: Characterization of Retrievals and First Results from a  
1032 Novel Optical Design Instrument at a New NDACC Complementary Station, *J. Atmos. Ocean. Technol.*, 24(3),  
1033 432–448, doi:10.1175/JTECH1962.1, 2007.  
1034  
1035 Wood, S. W.: Validation of version 5.20 ILAS HNO<sub>3</sub>, CH<sub>4</sub>, N<sub>2</sub>O, O<sub>3</sub>, and NO<sub>2</sub> using ground-based  
1036 measurements at Arrival Heights and Kiruna, *J. Geophys. Res.*, 107(D24), 8208, doi:10.1029/2001JD000581,  
1037 2002.  
1038  
1039 Zhu, L., Henze, D. K., Cady-Pereira, K. E., Shephard, M. W., Luo, M., Pinder, R. W., Bash, J. O. and Jeong, G.  
1040 R.: Constraining U.S. ammonia emissions using TES remote sensing observations and the GEOS-Chem adjoint  
1041 model, *J. Geophys. Res. Atmos.*, 118(8), 3355–3368, doi:10.1002/jgrd.50166, 2013.  
1042

## Tables

**Table 1** FTIR stations used in the analysis. The location, longitude, latitude and altitude are given for each station as well as the instrument used for the measurements. Typical emission sources are mentioned in the station specifics tab. The topography describes ~~the topography~~ the geography of the region surrounding the site. N gives the number of observations made during the period of interest. Time period gives the period from which data is used. The last column describes the used algorithm for the retrieval.

Station Location	Lon	Lat	Altitude (m.a.s.l.)	Instrument	Station specifics	Topography	Time period	N	Retrieval type
Bremen, Germany	8.85E	53.10N	27	Bruker 125 HR	City, fertilizers, livestock	Flat	2008-2015	278	Normal
Toronto, Canada	79.60W	43.66N	174	ABB Bomem DA8	City, fertilizers, biomass burning	On the edge of lake Ontario	2008-2015	1167	Normal
Boulder, United States	105.26W	39.99N	1634	Bruker 120 HR	Fertilizers, biomass burning, livestock	Mountain range to the west	2010-2015	440	Normal
Tsukuba, Japan	140.13E	36.05N	31	Bruker 125 HR	Fertilizers, city	Mostly flat, hills to the north	2014-2015	66	Normal
Pasadena, United States	118.17W	34.20N	460	MKIV_JPL	City, fertilizers, biomass burning	Mountain range to the east	2010-2015	695	Normal
Mexico City, Mexico	99.18W	19.33N	2260	Bruker Vertex 80	City, fires, fertilizers	In between mountain ranges	2012-2015	3980	Normal
St-Denis, Reunion	55.5E	20.90S	85	Bruker 120 M	Fertilizers, biomass burning, remote	Volcanic	2008-2012	948	Wide
Wollongong, Australia	150.88E	34.41S	30	Bruker 125 HR	Fertilizers, biomass burning, low emissions	Coastal, hills to the west	2008-2015	3641	Wide
Lauder, New Zealand	169.68E	45.04S	370	Bruker 120 HR	Fertilizers, livestock	Hills	2008-2015	1784	Normal

**Table 2** Applied data filters to the IASI-NH<sub>3</sub> product.

Filter	Filter Criteria
Elevation	$ FTIR_{station} - IASI_{Observation}  < 300$ m
Thermal Contrast	Thermal contrast $> 12$ K
Surface Temperature	$T > 275.15$ K
IASI-NH <sub>3</sub> retrieval Error	None
Cloud cover fraction	$< 10\%$
Spatial sampling difference	$50_{km} \rightarrow 10_{km}$ , $\Delta x = 5$ km
Temporal sampling difference	$< 90$ minutes

Table 3. Summarized results of the comparison between FTIR-NH<sub>3</sub> and IASI-NH<sub>3</sub> total columns within the coincidence criteria threshold (xdiff < 25 km, tdiff < 90minutes). **N** is the number of averaged total columns, **MRD** is the Mean Relative Difference (in %), **r** and **slope** are the correlation coefficient and slope of the linear regression.

Sites	N	MRD in % (rms 1σ)	r	slope
Bremen	53	-22.5±(54.0)	0.83	0.60
Toronto	170	-46.0±(47.0)	0.79	0.84
Boulder	38	-38.2±(43.5)	0.76	1.11
Tsukuba	15	-28.3±(35.6)	0.67	0.57
Pasadena	16	-47.9±(30.1)	0.59	0.83
Mexico	65	-30.8±(43.9)	0.64	1.14
St.-Denis	20	-61.3±(78.7)	0.65	1.26
Wollongong	62	6.0±(74.3)	0.47	0.92
Lauder	108	-29.7±(57.3)	0.55	0.77
<b>Combined</b>	<b>547</b>	<b>-32.4±(56.3)</b>	<b>0.80</b>	<b>0.73</b>

Figures

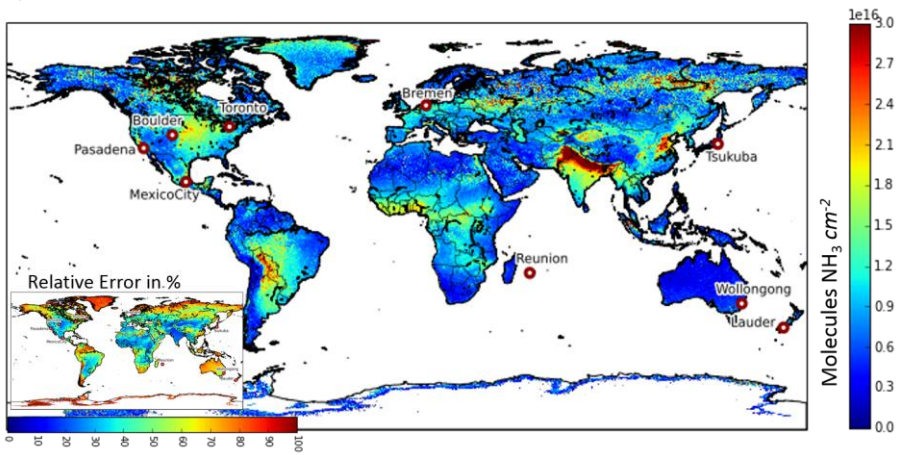


Figure 1. Mean IASI-NH<sub>3</sub> total column distribution for the period between January 2008 and January 2015. The total columns are a weighted average of the individual observations weighted with the relative error. Red circles indicate the positions of the FTIR stations.

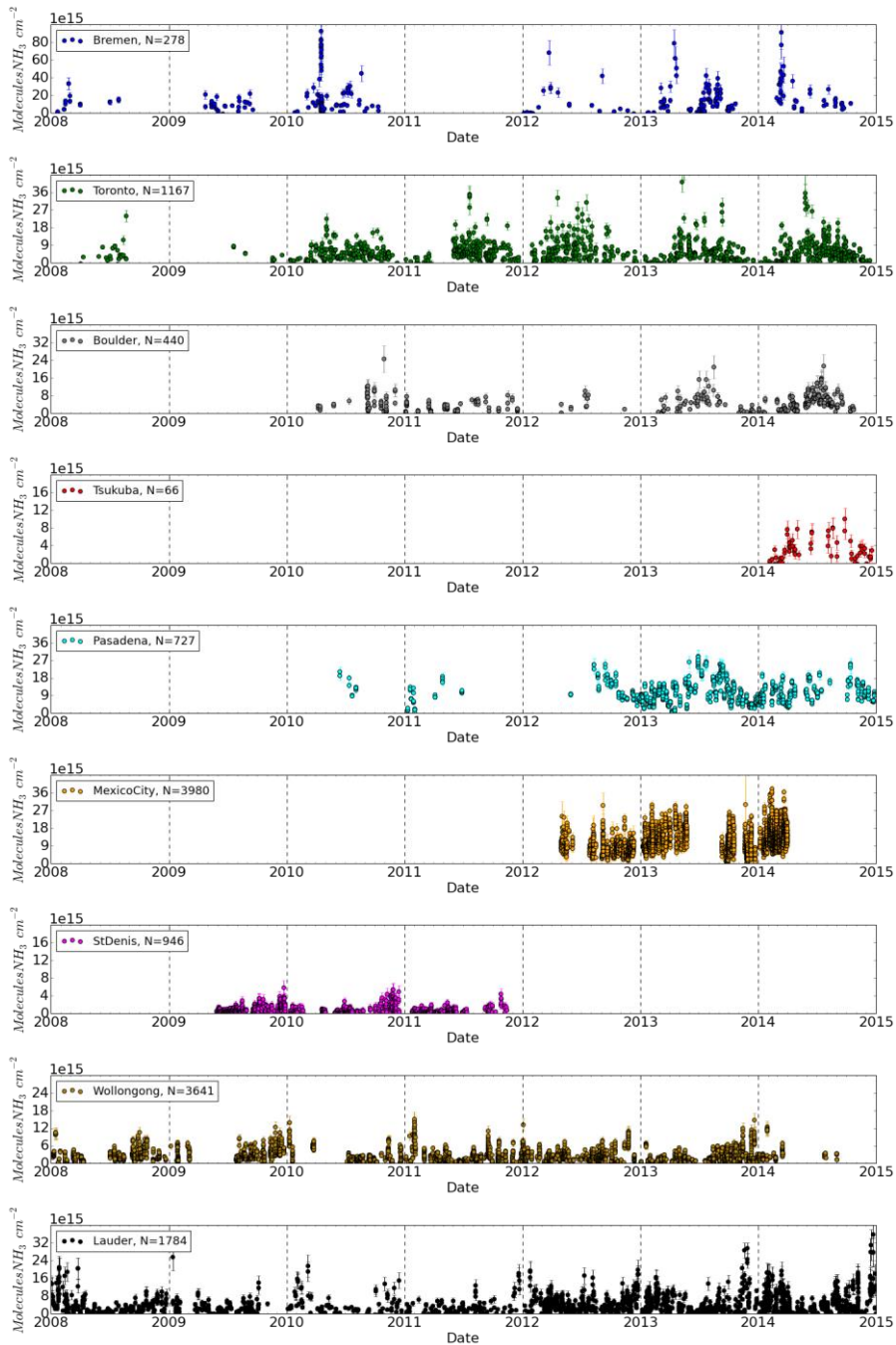


Figure 2. FTIR retrieved NH<sub>3</sub> Total Columns (in *molecules cm<sup>-2</sup>*). Note, the labels on the vertical axis vary for each site.



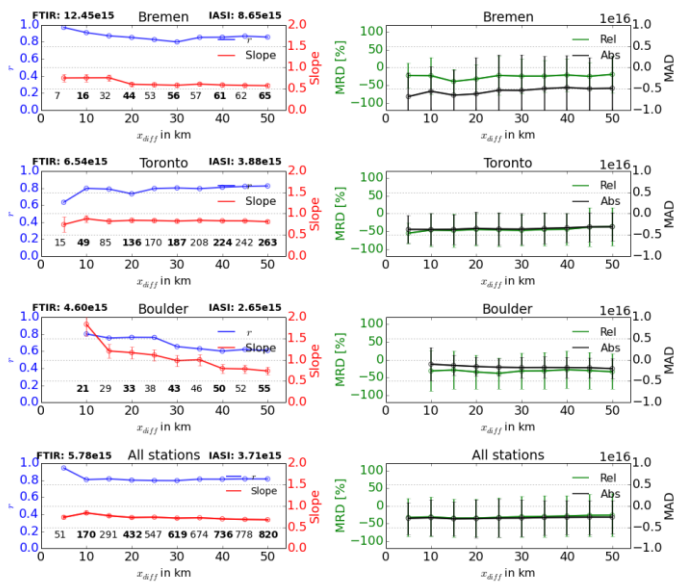


Figure 3. Correlation  $r$  (Blue lines, left figures), slope (Red lines, left figures) regression results, Mean Relative Difference (MRD, green lines, right figures) and Mean Absolute Difference (MAD, black lines, right figures) between IASI and FTIR observations as a function of  $x_{diff}$  for a selection of sites. Bars indicate the standard deviation of the slope of the individual regression results. The numbers in the bottom of each subplot show the number of matching observations. The numbers on the left and right side of the stations name give the mean FTIR and IASI total columns for  $x_{diff} < 25$  km.

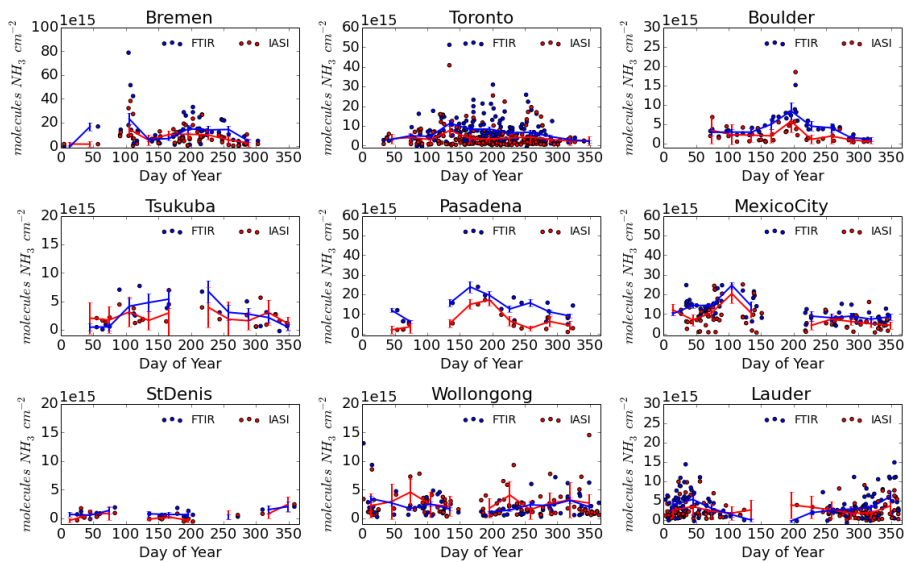


Figure 4. Time series of  $\text{NH}_3$  for IASI and FTIR datasets with  $\text{xdiff} < 25 \text{ km}$  and  $\text{tdiff} < 90 \text{ minutes}$  (FTIR: Blue and IASI: Red). Scattered values are the observations for each day of year (multiple years of observations). The lines show the monthly mean total columns of the respective sets.

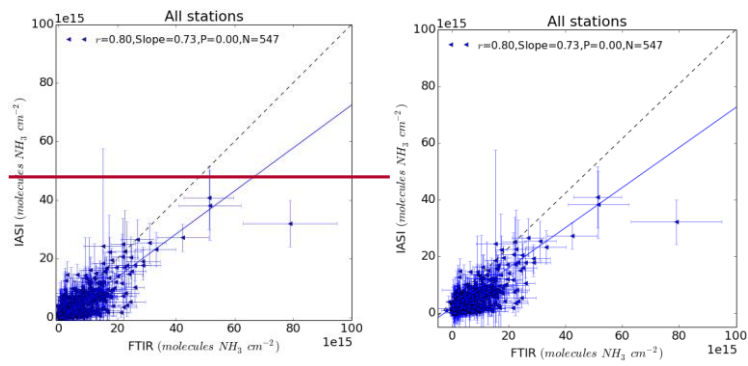


Figure 5. Correlations between the FTIR and IASI total columns with filters thermal contrast  $> 12 \text{ K}$ ,  $\text{tdiff} < 90 \text{ min}$ ,  $\text{xdiff} < 25 \text{ km}$ . The trend line shows the results of the regression analysis.

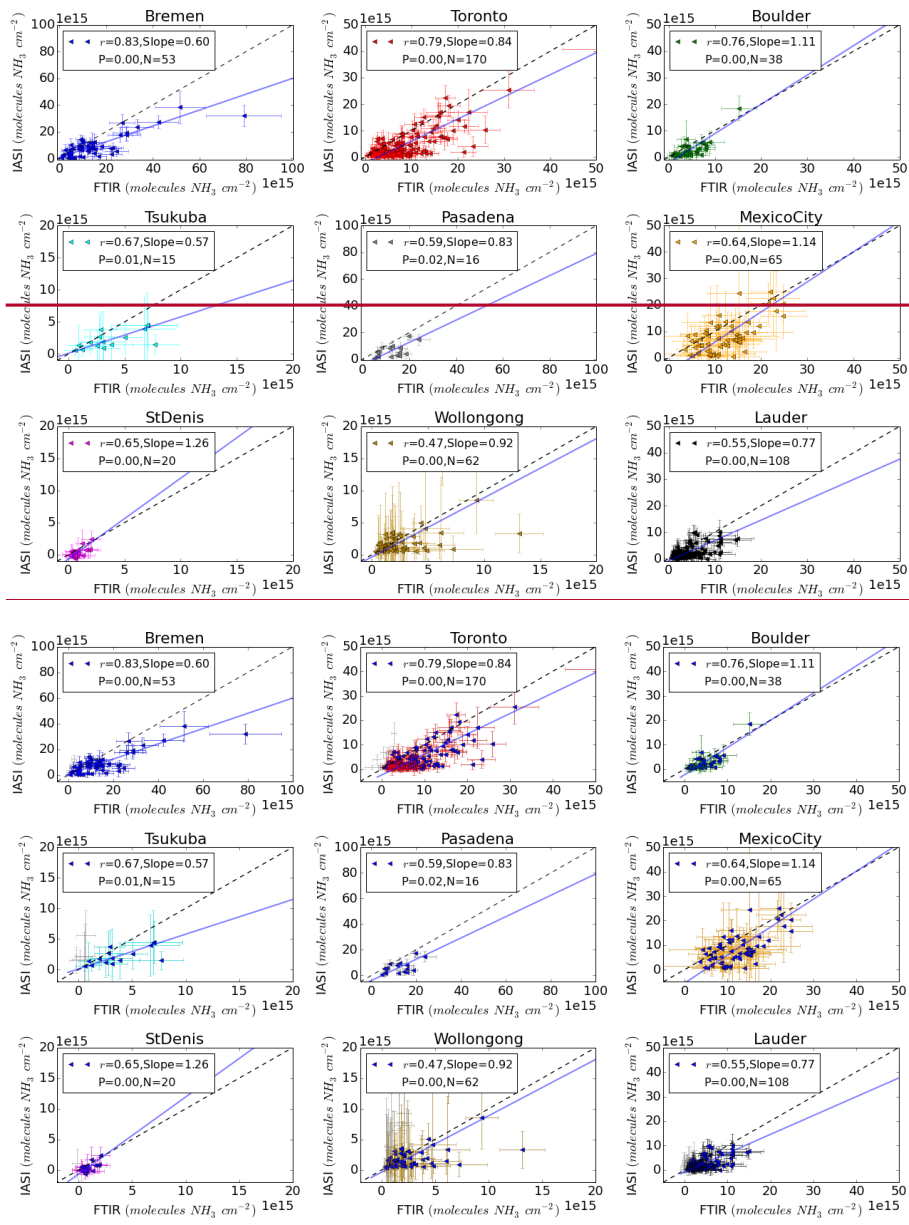


Figure 6. Correlations between the FTIR and IASI total columns with filters thermal contrast > 12, tdiff < 90min, xdiff < 25\_km. The trend lines show the results of the regression analysis.

Appendix A

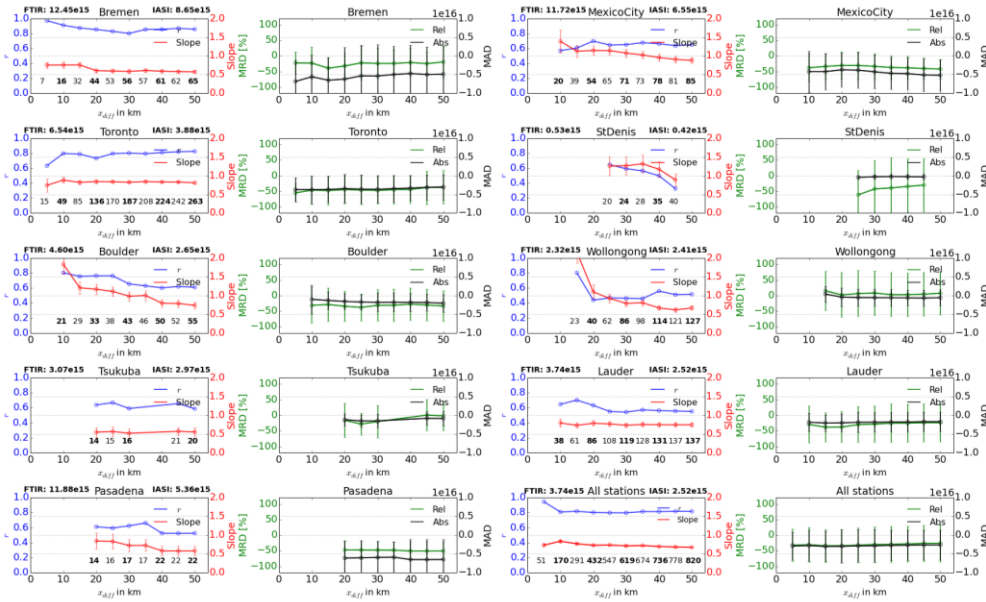


Figure A1. Correlation  $r$  (Blue lines, left figures), slope (Red lines, left figures) regression results, Mean Relative Difference (MRD, green lines, right figures) and Mean Absolute Difference (MAD, black lines, right figures) between IASI and FTIR observations as a function of  $x_{diff}$  for all sites. Bars indicate the standard deviation of the slope of the individual regression results. The numbers on the bottom of each subfigure show the number of matching observations. The numbers on the left and right side of the stations name give the mean FTIR and IASI total columns for a  $x_{diff} < 25$  km.

This section further covers the other stations, in addition to the sites covered by section 3.1. The results for Mexico City show an overall constant correlation coefficient except for small criteria  $< 20$  km. The slope also decreases towards values seen at other stations. This effect could be due to a large number of sources inside the city, i.e. automobile and agricultural emissions in and near the city, increasing the heterogeneity of the found column totals. Reunion and Tsukuba have few coincident observations leading to only a few significant comparisons. This, combined with the low concentrations measured at Reunion leads to large differences in the mean and standard deviations of the subsequent  $x_{diff}$  sets. The Reunion and Wollongong observations are at the sensitivity limit of the IASI-NH<sub>3</sub> retrieval which limits the usefulness of the sites for the validation. As there are only a few observations for Tsukuba it is hard to make meaningful conclusions for the variability around the site.